

Video Super Resolution Based on Deep Learning: A comprehensive survey

Hongying Liu, *Member, IEEE*, Zhubo Ruan, Peng Zhao, Fanhua Shang, *Senior Member, IEEE*,
Linlin Yang, Yuanyuan Liu, *Member, IEEE*

Abstract—In recent years, deep learning has made great progress in the fields of image recognition, video analysis, natural language processing and speech recognition, including video super-resolution tasks. In this survey, we comprehensively investigate 28 state-of-the-art video super-resolution methods based on deep learning. It is well known that the leverage of information within video frames is important for video super-resolution. Hence we propose a taxonomy and classify the methods into six sub-categories according to the ways of utilizing inter-frame information. Moreover, the architectures and implementation details (including input and output, loss function and learning rate) of all the methods are depicted in details. Finally, we summarize and compare their performance on some benchmark datasets under different magnification factors. We also discuss some challenges, which need to be further addressed by researchers in the community of video super-resolution. Therefore, this work is expected to make a contribution to the future development of research in video super-resolution, and alleviate understandability and transferability of existing and future techniques into practice.

Index Terms—Video Super-resolution, Deep Learning, Convolutional Neural Network, Inter-frame Information.

I. INTRODUCTION

Super-resolution (SR) aims at recovering a high-resolution (HR) image or multiple images from the corresponding low-resolution (LR) counterparts. It is a classic and challenging problem in computer vision and image processing, and it has extensive real-world applications, such as medical image reconstruction, face, remote sensing and panorama video super-resolution, video surveillance and high-definition television. With the advent of the 5th generation mobile communication technology, larger size images or videos can be transformed within a shorter time. Meanwhile, with the popularity of high definition (HD) and ultra high definition (UHD) display devices, super-resolution is attracting more and more attention.

Video is one of the most common multimedia in our daily life, and thus super-resolution of low-resolution videos has become very important. In general, image super-resolution methods process a single image at a time, while video super-resolution algorithms deal with

multiple successive images/frames at a time so as to utilize relationship information within frames to resolve the target frame. In a broad sense, video super-resolution can be regarded as image super-resolution and is able to be processed by image super-resolution algorithms frame by frame. However, the results are always not satisfactory as artifacts and jams may be brought in, which causes unguaranteed temporal coherence within frames.

In recent years, many video super-resolution algorithms have been proposed. They mainly fall into two categories: the traditional methods and deep learning based methods. For instance, as a traditional method, Liu and Sun[1] proposed a Bayesian approach to simultaneously estimate underlying motion, blur kernel, and noise level and reconstruct high-resolution frames. In [2], the expectation maximization (EM) method is adopted to estimate the blur kernel, and guide the reconstruction of high-resolution frames. However, these explicit models of high-resolution videos are still inadequate to fit various scenes in videos due to their fixed solution. With the great success of deep learning in a variety of area, super-resolution algorithms based on deep learning are studied extensively. Many deep neural networks (such as convolutional neural network (CNN), generative adversarial network (GAN) and recurrent neural network (RNN)) based video super-resolution methods have been proposed. Generally, they employ a large number of both low-resolution and high-resolution video sequences to input the neural network for inter-frame alignment, feature extraction/fusion and training the network, and then to product the high-resolution (HR) sequences for the corresponding low-resolution (LR) video sequences. The process flowchart of most video super-resolution methods mainly includes one alignment module, one feature extraction and fusion module, and one reconstruction module, as shown in Fig. 1. Because of the nonlinear learning capability of deep neural networks, the deep learning based methods usually achieve good performance on many public benchmark datasets.

There are few works about the overview on video super-resolution tasks, though many works [3, 4, 5] on the investigation of single image super-resolution have been published. Daithankar and Ruikar [6] presented a brief review on many frequency-spatial domain methods, nevertheless the deep learning methods are rarely mentioned. Unlike previous works, we provide a com-

H. Liu, Z. Ruan, P. Zhao, F. Shang, L. Yang and Y. Liu are with the Key Laboratory of Intelligent Perception and Image Understanding of Ministry of Education, School of Artificial Intelligence, Xidian University, China. E-mails: {hyliu, fhshang, yyliu}@xidian.edu.cn.

Manuscript received July 21, 2020.

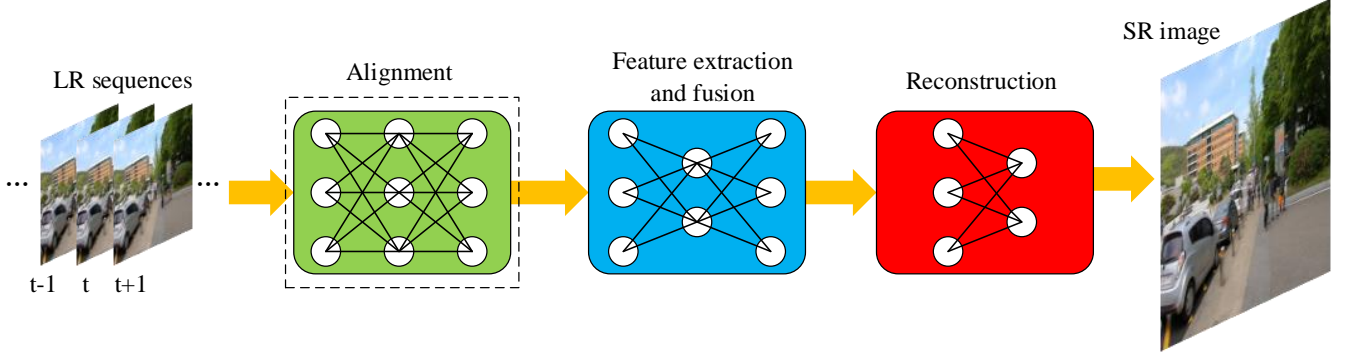


Fig. 1: The general flowchart of deep learning methods for video super-resolution. Note that the inter-frame alignment module can be either traditional methods or deep convolution neural networks, while both the feature extraction & fusion module and the upsampling module usually utilize deep convolution neural networks. The dashed line box means that the module is optional.

prehensive investigation on deep learning techniques for video super-resolution in recent years. It is well known that the main difference between video super-resolution and image super-resolution lies in the processing of information within frames. And the effective leverage information from nearby frames is critical for super-resolution results. We focus on the ways of utilizing information within frames for various deep learning based methods.

The contributions of this work are mainly summarized as follows. 1) We review recent work and progress on developing techniques for deep learning based video super-resolution. 2) We propose a taxonomy for deep learning based video super-resolution methods by categorizing their utilization ways of inter-frame information and illustrate how the taxonomy can be used to categorize existing methods. 3) We summarize the performance of state-of-the-art methods on some public benchmark datasets. 4) We also analyze some challenges and perspectives for video super-resolution tasks.

The rest of the paper is organized as follows. In Section 2, we briefly introduce the background of video super-resolution. In Section 3, we describe each method in details according to the taxonomy. In Section 4, the performance of state-of-the-art methods is analyzed quantitatively. In Section 5, we discuss the challenges and prospective trends in video super-resolution. Finally, we conclude this work in Section 6.

II. BACKGROUND

Video super-resolution stems from image super-resolution, and they aim at restoring high-resolution (HR) images/videos from one or more low-resolution (LR) observations. However, the difference between video and image super-resolution techniques is also obvious, that is, the former usually takes advantage of inter-frame information. Let \hat{I} denote a low-resolution video frame, and I be a high-resolution video frame.

Then the degradation process of HR video sequences can be formulated as follows:

$$\hat{I} = \phi(I; \theta_\alpha) \quad (1)$$

where $\phi(\cdot; \cdot)$ denotes the degradation function, and θ_α denotes the parameters of the degradation function and represents various degradation factors, such as noise, motion blur, downsampling factors. In practice, it is easy to obtain \hat{I} , but the degradation factors which may be quite complex or is probably a combination of several factors are unknown. Video super-resolution aims at solving the degraded video sequences and thus recovering the corresponding HR video sequences, and makes them as close to the ground truth (GT) video as possible. The super-resolution process, namely the reverse process of Eq. (1), can be formulated as follows:

$$\tilde{I} = \phi^{-1}(\hat{I}; \theta_\beta) \quad (2)$$

where \tilde{I} denotes the estimation of the GT (i.e., I).

In most existing methods, the degradation process is modeled as:

$$\hat{I} = (I \otimes k) \downarrow_s + n \quad (3)$$

where k denotes the blur kernel, n is Gaussian noise, \downarrow_s and \otimes represent the downsampling with scale s and convolution, respectively.

Like image super-resolution, video quality is mainly evaluated by calculating peak signal-noise ratio (PSNR) and structural similarity index (SSIM). These indexes measure the difference of pixels and the similarity of structure between two images, respectively. PSNR is defined as:

$$\text{PSNR} = 10 \log_{10} \left(\frac{L^2}{\text{MSE}} \right) \quad (4)$$

$$\text{MSE} = \frac{1}{N} \sum_{i=1}^N (I(i) - \tilde{I}(i))^2 \quad (5)$$

where L represents the maximum range of color value, which is usually 255, N denotes the total number of

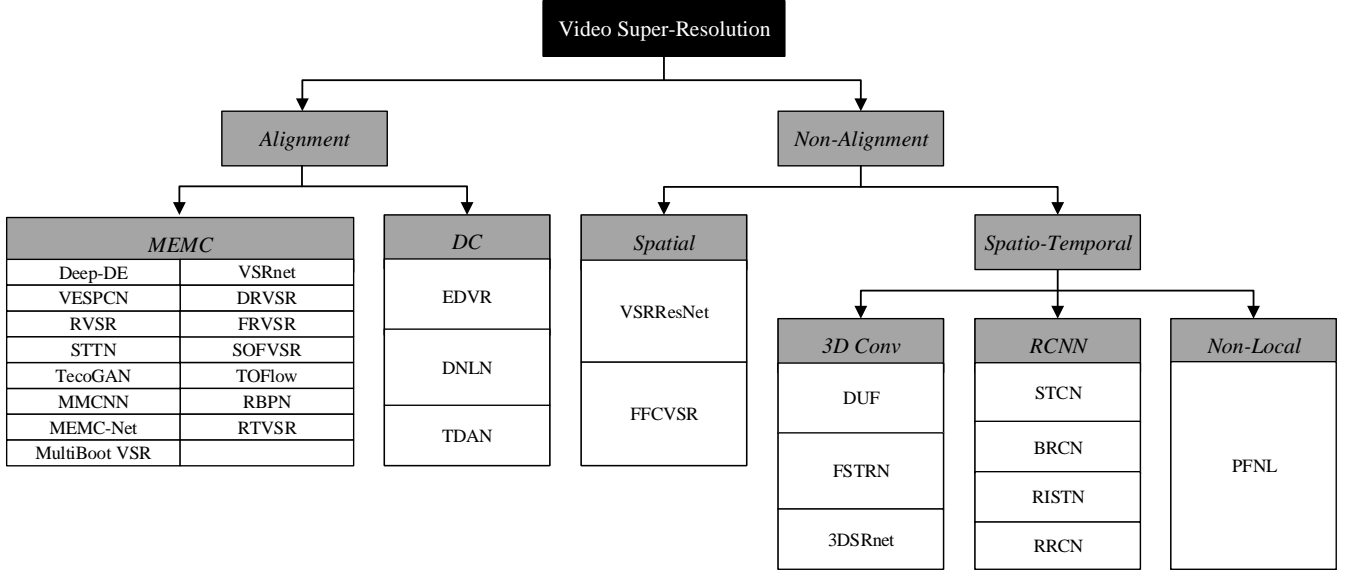


Fig. 2: A taxonomy for existing state-of-the-art video super-resolution methods. Here, *MEMC* stands for motion estimation and compensation methods, *DC* is deformable convolution methods, *3D Conv* is 3D convolution methods, and *RCNN* denotes recurrent convolutional neural networks.

pixels in an image. A higher value of PSNR generally means superior quality.

SSIM is defined as:

$$\text{SSIM}(I, \tilde{I}) = \frac{2u_I u_{\tilde{I}} + k_1}{u_I^2 + u_{\tilde{I}}^2 + k_1} \cdot \frac{2\sigma_{I\tilde{I}} + k_2}{\sigma_I^2 + \sigma_{\tilde{I}}^2 + k_2} \quad (6)$$

where u_I and $u_{\tilde{I}}$ represent the mean value of the image I and \tilde{I} , respectively. k_1 and k_2 are constants, which are used to stabilize the calculation and are usually set to 0.01 and 0.03, respectively. σ_I and $\sigma_{\tilde{I}}$ denote the standard deviations, and $\sigma_{I\tilde{I}}$ denotes the covariance. They are defined as:

$$u_I = \frac{1}{N} \sum_{i=1}^N I(i) \quad (7)$$

$$\sigma_I = \left[\frac{1}{N-1} \sum_{i=1}^N (I(i) - u_I)^2 \right]^{\frac{1}{2}} \quad (8)$$

$$\sigma_{I\tilde{I}} = \frac{1}{N-1} \sum_{i=1}^N (I(i) - u_I)(\tilde{I}(i) - u_{\tilde{I}}). \quad (9)$$

Moreover, considering the characteristics of video sequences, several measurements have been proposed and used for the evaluation of recovered video quality, including MOVIE [7, 8], Learned Perceptual Image Patch Similarity (LPIPS) [9] and the two measurements: tOF and tLP, which were proposed in [10].

III. VIDEO SUPER-RESOLUTION METHODS

As the videos are a recording of moving visual images and sound, the methods for video super-resolution learn from existing single image super-resolution methods. There are many deep learning based image super-resolution methods, such as SRCNN [37], and its improved variants: FSRCNN [38], VDSR [39], ESPCN [40],

RDN [41], RCAN [42], ZSSR [43] and SRGAN [44]. In 2016, based on SRCNN, Kappeler [12] presented a video super-resolution method with convolutional neural networks (VSRnet), which is a well-known method that applies deep learning to video super-resolution tasks. So far, many video super-resolution algorithms have been proposed. In the following, we summarize the characteristics of deep learning based methods for video super-resolution in recent years, as shown in Table I.

Several papers such as [24, 29, 26] on video super-resolution have indicated that the utilization of information between frames greatly influences performance. And proper and adequate usage of such information can enhance the results of super-resolution. Therefore, we build a taxonomy for existing video super-resolution methods according to their ways of the utilization of inter-frame information, as shown in Fig. 2.

As shown in Fig. 2 and Table I, we categorize the existing methods into two main categories: aligned and non-aligned methods, according to whether the video frames are aligned. We will present these methods in details in the following sections.

IV. ALIGNED METHODS

The aligned methods make neighboring frames align with the target frame by using extracted motion information through networks before subsequent reconstruction. And the methods mainly use motion compensation or deformation convolution, which are two common techniques for aligning frames. Next we will introduce state-of-the-art methods based on each of the techniques in details.

TABLE I: Existing video super-resolution methods based on deep learning and their key strategies. Here, *MEMC* stands for motion estimation and compensation methods, *DC* is deformable convolution methods, *3D Conv* is 3D convolution methods, and *RCNN* denotes recurrent convolutional neural networks.

Method	Year	Title	Type	Keywords	Alignment
Deep-DE [11]	2015	Video Super-Resolution via Deep Draft-Ensemble Learning	MEMC	SR draft ensemble generation	✓
VSRnet [12]	2016	Video Super-Resolution with Convolutional Neural Networks		deep learning, deep neural networks, convolutional neural networks	✓
RVSR [13]	2017	Robust Video Super-Resolution with Learned Temporal Dynamics		temporal adaptive neural network, spatial alignment network	✓
DRVSR [14]	2017	Detail-Revealing Deep Video Super-Resolution		sub-pixel motion compensation	✓
VESPCN [8]	2017	Real-Time Video Super-Resolution with Spatio-Temporal Networks and Motion Compensation		real-time, spatio-temporal sub-pixel convolution, fast multi-resolution spatial transformer	✓
TecoGAN [10]	2018	Learning Temporal Coherence via Self-Supervision for GAN-based Video Generation		generative adversarial network, temporal cycle-consistency, self-supervision, unpaired video translation	✓
STTN [15]	2018	Spatio-Temporal Transformer Network for Video Restoration		spatio-temporal transformer network	✓
FRVSR [16]	2018	Frame-Recurrent Video Super-Resolution		frame-recurrent	✓
SOFVSR [17]	2018	Learning for Video Super-Resolution through HR Optical Flow Estimation		HR Optical Flow Estimation	✓
MMCNN [18]	2019	Multi-memory Convolutional Neural Network for Video Super-Resolution		long short-term memory, multi-memory residual block	✓
MEMC-Net [19]	2019	Memc-net: Motion Estimation and Motion Compensation Driven Neural Network for Video Interpolation and Enhancement		Adaptive Warping	✓
MultiBoot VSR [20]	2019	Multiboot VSR: Multi-Stage Multi-Reference Bootstrapping for Video Super-Resolution		recurrent structure	✓
RTVSR [21]	2019	Real-Time Video Super-Resolution via Motion Convolution Kernel Estimation		motion convolution kernel estimation	✓
TOFlow [22]	2019	Video Enhancement with Task-Oriented Flow		task-oriented flow, Vimeo90K dataset	✓
RBPNet [23]	2019	Recurrent Back-Projection Network for Video Super-Resolution		iterative refinement, multiple projection	✓
EDVR [24]	2019	Video Restoration with Enhanced Deformable Convolutional Networks	DC	large motion handling, Pyramid Cascading and Deformable alignment, Temporal and Spatial Attention fusion	✓
DNLN [25]	2019	Deformable Non-Local Network for Video Super-Resolution		deformable convolution, non-local operation	✓
TDAN [26]	2020	TDAN: Temporally-Deformable Alignment Network for Video Super-Resolution		dynamic kernel offsets prediction	✓
FFCVSR [27]	2019	Frame and Feature-Context Video Super-Resolution	Spatial	frame and feature-context	×
VSRResNet [28]	2019	Generative Adversarial Networks and Perceptual Losses for Video Super-Resolution		generative adversarial network, perceptual loss	×
DUF [29]	2018	Deep Video Super-Resolution Network Using Dynamic Upsampling Filters without Explicit Motion Compensation	3D conv	dynamic upsampling filters	×
BRCN [30]	2018	Video Super-Resolution via Bidirectional Recurrent Convolutional Networks		recurrent neural networks, 3D convolution	×
3DSRnet [31]	2019	Video Super-Resolution Based on 3D-CNNs with Consideration of Scene Change		3D convolution	×
FSTRN [32]	2019	Fast Spatio-Temporal Residual Network for Video Super-Resolution		3D convolution decomposition	×
STCN [33]	2017	Building an End-to-End spatio-temporal Convolutional Network for Video Super-Resolution	RCNN	spatio-temporal network	×
BRCN [30]	2018	Video Super-Resolution via Bidirectional Recurrent Convolutional Networks		recurrent neural networks, 3D convolution	×
RRCN [34]	2019	Video Super-Resolution using Non-Simultaneous Fully Recurrent Convolutional Network		non-simultaneous, residual connection, model ensemble	×
RISTN [35]	2019	Residual Invertible Spatio-Temporal Network for Video Super-Resolution		lightweight residual invertible block, recurrent convolutional model with residual dense connections, sparse strategy	×
PFNL [36]	2019	Progressive Fusion Video Super-Resolution Network via Exploiting Non-local Spatio-Temporal Correlations	Non-local	improved non-local operation	×
DNLN [25]	2019	Deformable Non-Local Network for Video Super-Resolution		deformable convolution, non-local operation	✓



Fig. 3: An example of motion estimation and compensation. Note that the rightmost image is the legend of (d), where different colors represent different directions of motion and the intensity of the color denotes the range of motion.

A. Motion Estimation and Compensation Methods

In the aligned methods for video super-resolution, most methods apply the motion compensation and motion estimation techniques. Specifically, the purpose of motion estimation is to extract inter-frame motion information, while motion compensation is used to perform the warp operation between frames according to inter-frame motion information and to make one frame align with another frame. A majority of the motion estimation techniques are performed by the optical flow method [45]. This method tries to calculate the motion between two neighboring frames through their correlations and variations in the temporal domain. The motion compensation methods can be divided into traditional methods (such as the LucasKanade [46] and Druleas [47] algorithms) and deep learning methods, such as FlowNet [45], FlowNet 2.0 [48] and SpyNet [49].

In general, an optical flow method takes two consecutive frames (i.e., I_i and I_j) as input, where one is the target frame and the other is the neighboring frame. Then the method computes a vector field of optical flow $F_{i \rightarrow j}$ from the frame I_i to I_j by the following formula:

$$F_{i \rightarrow j} = (h_{i \rightarrow j}, v_{i \rightarrow j}) = ME(I_i, I_j; \theta_{ME}) \quad (10)$$

where $h_{i \rightarrow j}$ and $v_{i \rightarrow j}$ is the horizontal and vertical components of $F_{i \rightarrow j}$, $ME(\cdot)$ is a function used to compute optical flow and θ_{ME} is its parameter.

The motion compensation is used to perform image transformation between images in terms of motion information to make neighboring frames align with the target

frame spatially. It can be achieved by some methods, such as bilinear interpolation and spatial transformer network (STN) [50]. In general, a compensated frame J is expressed as:

$$J = MC(I, F; \theta_{ME}) \quad (11)$$

where $MC(\cdot)$ denotes a motion compensation function, I , F and θ_{ME} are the neighboring frame, optical flow and the parameter, respectively. An example of the motion estimation and motion compensation is shown in Fig. 3. Below we depict some representative methods in this category.

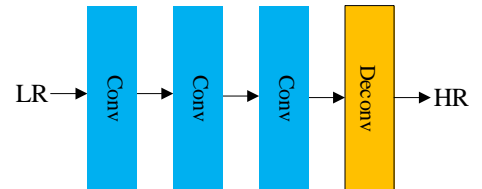


Fig. 4: The network architecture of Deep-DE [11], where Conv denotes a convolutional layer and Deconv denotes a deconvolutional layer.

1) *Deep-DE¹*: The deep draft-ensemble learning method (Deep-DE) [11], as illustrated in Fig. 4, has the following four major phases. It first generates a series of SR drafts by adjusting the TV- ℓ_1 loss [51, 52] and the motion detail preserving (MDP) [53]. Then both

¹Code: <http://www.cse.cuhk.edu.hk/leojia/projects/DeepSR/>

the SR drafts and the bicubic-interpolated LR target frame are fed into a convolutional neural network to perform feature extraction, fusion and super-resolution operations.

The convolutional neural network consists of four convolutional layers, where the first three layers are general convolutional layers, and the last layer is a de-convolution layer. Their kernel sizes are 11×11 , 1×1 , 3×3 and 25×25 , respectively, and the numbers of channels is 256, 512, 1 and 1. Deep DE uses the ℓ_1 -norm loss with a total variation regularization as its loss function.

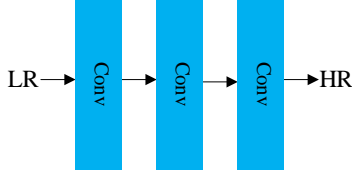


Fig. 5: The network architecture of VSRnet [12], where Conv denotes a convolutional layer.

2) *VSRnet*²: VSRnet [12] is based on the image super-resolution method, SRCNN [37], and its network architecture is shown in Fig. 5. It consists of three convolutional layers, and each convolutional layer is followed by a rectified linear unit (ReLU) except for the last one. The main difference between VSRnet and SRCNN is the number of input frames. That is, SRCNN takes a single frame as input, while VSRnet uses multiple successive frames, which are compensated frames. The motion information between frames is computed by the Druleas algorithm [47]. In addition, VSRnet proposes a filter symmetry enforcement (FSE) mechanism and an adaptive motion compensation mechanism, which are separately used to accelerate training and reduce the impact of unreliable compensated frames, and thus can improve video super-resolution performance.

VSRnet adopts the Myanmar³ videos as the training dataset, whose resolution is $3,840 \times 2,160$. In the experiment, the ground truth videos are collected by down-sampling original videos to the resolution of 960×540 . LR videos are obtained by performing a bicubic interpolation. More specially, the input frames are upsampled before feeding into the network and the number of input frames is 5. Then the frames are converted to the YCbCr color space, where the Y channel is used for training the network and performance assessment. The testing set is the Vid4⁴ dataset, which consists of four common videos (city, calendar, walk and foliage). The numbers of frames for the four videos are 34, 41, 47, and 49, respectively, and their resolutions are 704×576 , 720×576 , 720×480 and 720×480 , respectively. The training strategy of VSRnet is that the pre-trained SRCNN is used to initialize the network weights in order to reduce the dependence on

large-scale video datasets. Then VSRnet is trained with small-scale video datasets. The loss function of VSRnet is the mean squared error (MSE) loss.

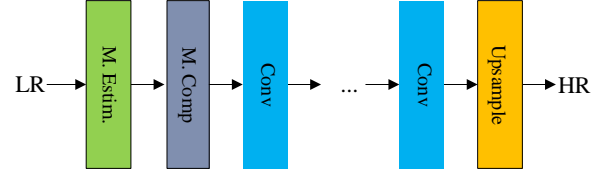


Fig. 6: The network architecture of VESPCN [8]. Here, M. Estim. denotes a motion estimation block, M. Comp denotes a motion compensation block, and Upsample denotes a sub-pixel convolutional layer.

3) *VESPCN*: The video efficient sub-pixel convolutional network (VESPCN) [8] proposes a spatial motion compensation transformer (MCT) module for motion estimation and compensation. Then the compensated frames are fed into a series of convolutional layers for feature extraction and fusion. Finally, super-resolution results are obtained through a sub-pixel convolutional layer. The network architecture of VESPCN is illustrated in Fig. 6.

The MCT module adopts convolutional neural networks to extract motion information and perform motion compensation. The module uses a coarse-to-fine approach to compute the optical flow for image sequences. Firstly, in the coarse estimation stage, the network takes two consecutive frames as input, where one frame is the target frame and the other is a neighboring frame. The coarse network consists of 5 convolutional layers and a sub-pixel convolutional layer. It first performs the $\times 2$ downsampling operation two times and then performs the $\times 4$ upsampling operation by a sub-pixel convolutional layer to get coarse optical flow estimation results. Secondly, the neighboring frame is warped according to the optical flow. In the fine estimation stage, the target frame, neighboring frame, optical flow computed at the coarse estimation stage and the warped neighboring frame are input to the network. The architecture of the fine network is the same as the coarse network. It first conducts $\times 2$ downsampling and then perform $\times 2$ upsampling at the end of the network to attain the fine optical flow. Then the coarse optical flow adds the fine optical flow to obtain the final estimation result. Finally, the neighboring frame is warped again by the final optical flow to make the warped frame align with the target frame.

VESPCN uses the videos collected from the CDVL database⁵ as the training dataset, which includes 115 videos with size $1,920 \times 1,080$, and Vid4 is used as the testing dataset. The LR videos are obtained by down-sampling from the HR videos. The number of input frames is set to 3. The loss function consists of both MSE and motion compensation loss, where the motion

²Code: <https://superresolution.tf.fau.de/>

³<https://www.harmonicinc.com/>

⁴<https://twitter.box.com/v/vespcn-vid4>

⁵<http://www.cdvl.org/>

compensation loss denotes the difference between the warped frame and the target frame. The network applies the Adam [54] optimizer for training. The batch size is 16, and the learning rate is set to 10^{-4} .

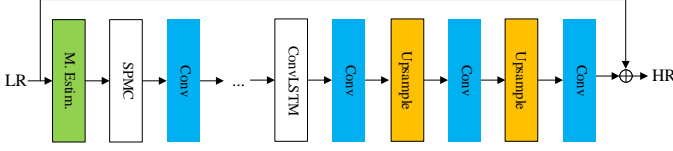


Fig. 7: The network architecture of DRVSR [14], where SPMC denotes a sub-pixel motion compensation layer, ConvLSTM is the convolutional LSTM [55], and \oplus denotes element-wise sum.

4) *DRVSR*⁶: The detail-revealing deep video super-resolution (DRVSR) [14] method proposes a sub-pixel motion compensation layer (SPMC) that can perform the up-sampling and motion compensation operation simultaneously for neighboring input frames according to the estimated optical flow information. Its network architecture is shown in Fig. 7.

DRVSR consists of three main modules: a motion estimation module, a motion compensation module, and a fusion module. For the motion estimation module, it adopts the motion compensation transformer (MCT) [8] for motion estimation, and adopts the SPMC layer for motion compensation. The SPMC layer consists of two sub-modules, namely grid generator and sampler. The grid generator first transforms the coordinates in the LR space into the coordinates in the HR space according to the optical flow, and then the sampler performs the interpolation operation in the HR space. The fusion module mainly includes an encoder and a decoder. In the encoder, it applies the convolution with stride 2 to perform down-sampling and then conducts the deconvolution to perform up-sampling. In addition, the fusion module also adopts the ConvLSTM module [55] to handle spatio-temporal information.

The training of DRVSR is divided into three stages. First of all, the motion estimation module is trained with its motion compensation loss. Then the parameters of the trained motion estimation module are fixed, and the fusion module is trained based on the MSE loss. Finally, the entire network is fine-tuned using the total loss of MSE and motion compensation loss. Moreover, in order to make training process stable, DRVSR adopts the gradient clip strategy to constrain the weight of ConvLSTM. Adam is used as the optimizer and the network weights are initialized by the Xavier [56], which is an efficient initialization method.

5) *RVSR*: The architecture of robust video super-resolution (RVSR) [13] is shown in Fig. 8. RVSR consists of a spatial alignment module and a temporal adaptive module. The spatial alignment module is responsible for

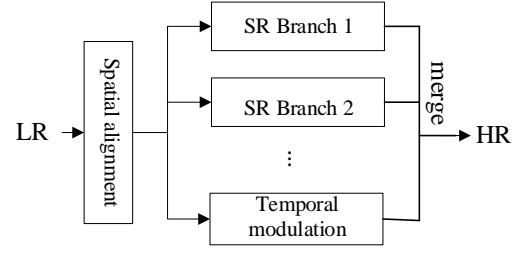


Fig. 8: The network architecture of RVSR [13].

the alignment of the multi-frames so that the neighboring frames are aligned with the target frame. It first estimates the transformation parameters between the neighboring frame and the target frame through a localization net, and then makes the neighboring frame align with the target frame through a spatial transformation layer [50] based on the obtained parameters. The localization net consists of two convolutional layers, each of which is followed by a max-pooling layer, and two fully connected layers. The feature of the temporal adaptive module is that it is composed of multiple branches of super-resolution subnetwork and each network is responsible for handling a temporal scale (i.e., the number of input frames), and outputting the corresponding super-resolution result. Then the super-resolution result of each branch network is allocated a weight through a temporal modulation module. The final super-resolution result is the weight sum of the super-resolution result of each branch and the corresponding weight. The input frame number of the temporal modulation module is identical to the maximum number of input frames in the super-resolution network, and the network structure of the temporal modulation module is the same as that of the super-resolution network, and both of them adopt the network structure of ESPCN [40].

RVSR uses the videos from the LIVE video quality assessment database, the MCL-V database, and the TUM 1080p dataset as the training set, and meanwhile employs data augmentation techniques. The Vid4, penguin (pg) [11], temple (tp) [11] and Ultra Video Group Database (UVGD)⁷ are adopted as the testing set. The number of input frames is 5, and the patch size is set to 30×30 . RVSR combines the loss of both the spatial alignment module and spatio-temporal adaptive module as the final loss function, in which the loss of the spatio-temporal adaptive module is the difference between the GT and the network output. And the loss of the spatial alignment module is the difference between the GT transformation parameters and transformation parameters estimated by the localization net, where the GT transformation parameters are obtained by the rectified optical flow alignment.

6) *FRVSR*⁸: The architecture of the frame recurrent video super-resolution (FRVSR) [16] method is illus-

⁶Code: https://github.com/jiangsutx/SPMC_VideoSR

⁷<http://ultravideo.cs.tut.fi/>

⁸Code: <https://github.com/msmsajjadi/FRVSR>

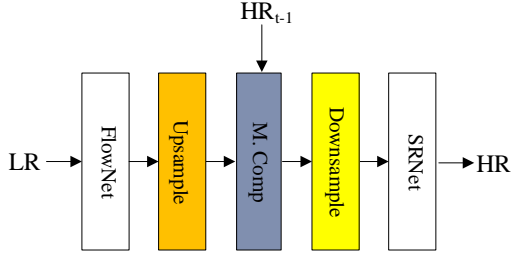


Fig. 9: The network architecture of FRVSR [16], where FlowNet is an optical estimation module, and SRNet is a super-resolution module.

trated in Fig. 9. Its main characteristic lies in the approach of alignment between frames. It does not warp the previous frame of the target frame directly, but warps the HR version of the previous frame. The detailed implementation way is that adopting an optical estimation network computes the optical flow from the previous frame to the target frame. Then the LR optical flow is upsampled to the same size with the HR video by bilinear interpolation. Next the HR version of the previous frame is warped by the upsampled LR optical flow, and then the warped HR frame is downsampled by space-to-depth transformation to get the LR version. Finally, the LR version of the warped HR frame and the target frame are fed into the subsequent super-resolution network to get the super-resolution result of the target frame.

In FRVSR, the optical flow network consists of 14 convolutional layers, 3 pooling layers and 3 bilinear upsampling layers. Each convolutional layer is followed by a LeakyReLU activation function, except for the last convolutional layer. The super-resolution network consists of 2 convolutional layers, 2 deconvolution layers with $\times 2$ and 10 residual blocks, where each residual block consists of 2 convolutional layers and a ReLU activation function. FRVSR adopts the combination of MSE and motion compensation loss as its loss function, Adam as the optimizer of the network and Vid4 as the testing set.

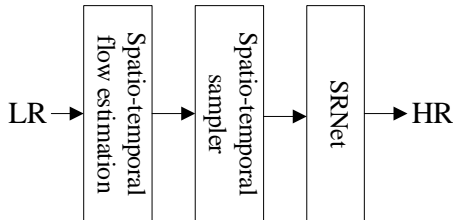


Fig. 10: The network architecture of STTN [15], where SRNet is a super-resolution module.

7) *STTN*: The architecture of the spatio-temporal transformer network (STTN) [15] is illustrated in Fig. 10. It proposes a spatio-temporal transformer module, which is used to solve the problem that previous optical flow methods only process a pair of video frames, which

may cause inaccurate estimation when occlusion and luminance variation exist in videos. The proposed module can handle multiple frames at a time, which overcomes the disadvantage of the methods.

STTN consists of three major modules: a spatio-temporal flow estimation module, a spatio-temporal sampler module, and a super-resolution module. The spatio-temporal flow estimation module is a U-style network, similar to U-Net [57], consisting of 12 convolutional layers and two up-sampling layers. It first performs $\times 4$ downsampling, and then performs $\times 4$ up-sampling to restore the size of the input frame. This module is responsible for the optical flow estimation of the consecutive input frames including the target frame and multiple neighboring frames, and the final output is a 3-channel spatio-temporal flow that expresses the spatial and temporal changes between frames. The spatio-temporal sampler module is actually a trilinear interpolation method, which is responsible for performing the warp operation for the current multiple neighboring frames and obtaining the aligned video frames according to the spatio-temporal flow obtained by the spatio-temporal flow module. For video super-resolution, the aligned frames can then be fed into the super-resolution network for feature fusion and super-resolution processing of the target frame. STTN adopts the combination of MSE and motion compensation loss as its loss function.

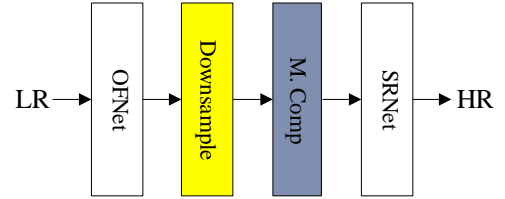


Fig. 11: The network architecture of SOFVSR [17], where OFNet is an optical flow network.

8) *SOFVSR*⁹: The architecture of super-resolution optical flow for video super-resolution (SOFVSR) [17] is shown in Fig. 11. The optical flow between frames is estimated by a coarse-to-fine approach including the optical flow network (OFNet), which finally yield a high-resolution optical flow. Then the HR optical flow is converted to the LR optical flow by a space-to-depth transformation. The neighboring frames are warped by the LR optical flow to make the neighboring frames align with the target frame. Then the super-resolution network (SRNet) takes the target frame and warped frames as input to obtain the final super-resolution result. SRNet consists of two convolutional layers, five residual dense blocks and a sub-pixel convolutional layer.

SOFVSR adopts 145 videos from the CDVL database³ as the training set, 7 videos from the Ultra Video Group database¹⁰ as the validation set, and Vid4 and 10 videos

⁹Code: <https://github.com/LongguangWang/SOF-VSR>

¹⁰ultravideo.cs.tut.f

from the DAVIS dataset [58] as the testing set. SOFVSR converts the RGB color space into the YCbCr color space and only uses the Y channel to train the network. The number of input frames is 3. Patch size is set to 32×32 , and data augmentation techniques are also used. The loss function includes the MSE and motion compensation loss, where the motion compensation loss includes three parts corresponding to three stages of OFNet, and each stage computes a motion compensation loss by using current optical flow. Adam is used as the optimizer for training the network. The initial learning rate is set to 10^{-4} and reduces by half after every 50K iterations.

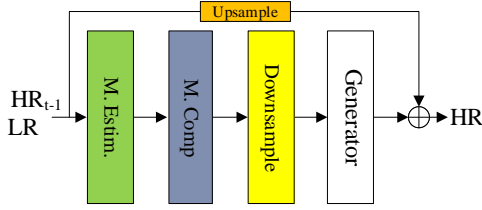


Fig. 12: The network architecture of TecoGAN [10].

9) *TecoGAN*¹¹: The architecture of the temporally coherent GAN (TecoGAN) [10] is also illustrated in Fig. 12. Like GAN, TecoGAN also consists of a generator and a discriminator. The generator takes the target frame, previous frame and previous estimated HR frame as input. First of all, input frames are fed into the optical flow module, which is a convolutional neural network similar to the optical flow estimation module in FRVSR [16]. In this module, the LR optical flow between the target frame and the neighboring frame is estimated, and it is used to enlarge the LR optical flow by the bicubic interpolation to attain the corresponding HR optical flow. Then the previous HR frame is warped by the HR optical flow. The warped previous HR frame and target frame are fed into subsequent convolutional layers to yield a restored target frame. Moreover, the discriminator assesses the quality of super-resolution results. The discriminator takes the generated results and GT as inputs, where the generated results and GT have three components, that is, three consecutive HR frames, three corresponding upsampled LR frames and three warped HR frames. With such input formats, the spatial over-smooth and temporal inconsistency in the final results can be relieved. In addition, TecoGAN also proposes a “ping-pong” loss function in order to reduce the long-term temporal detail drift and make super-resolution results more natural.

The loss function of TecoGAN consists of 6 parts including MSE, adversarial loss, feature space loss from discriminator, perceptual loss, “ping-pong” loss and motion compensation loss. Adam is used as the optimizer, Vid4 and Tear of Steel (ToS) are used as the testing set. Similar to other GAN-based methods, training makes the discriminator unable to distinguish whether the HR

image generated from the generator is a GT frame or synthetic super-resolution frame. Although these methods can yield HR videos with better perception quality, the PSNR value is usually relatively low, which may highlight the flaw of PSNR in assessing image and video quality.

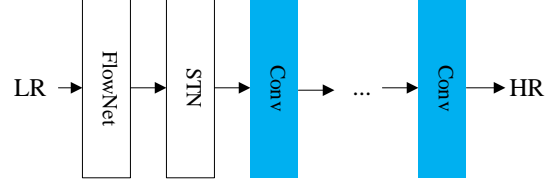


Fig. 13: The network architecture of TOFlow [22].

10) *TOFlow*¹²: The architecture of the task-oriented flow (TOFlow) [22] is shown in Fig. 13. TOFlow combines the network for optical flow estimation with the reconstruction network, and trains them jointly to obtain optical flow that is suitable for several tasks, such as video super-resolution, video interpolation, and video deblurring. TOFlow adopts SpyNet [49] as the network for the optical flow estimation, and then adopts a spatial transformer network to warp the neighboring frame according to the computed optical flow. Then the final result is obtained by the image processing module. For the video super-resolution task, the image processing module consists of 4 convolutional layers, where kernel sizes are 9×9 , 9×9 , 1×1 , and 1×1 , respectively, and the numbers of channels are 64, 64, 64, and 3, respectively.

TOFlow presents a new dataset, called Vimeo-90K (V-90K), for training and testing video sequences. V-90K consists of 4,278 videos including 89,800 different independent scenes. TOFlow adopts the L1-norm as its loss function. For video super-resolution, TOFlow takes 7 upsampled consecutive frames as input. Besides V-90K, TOFlow also uses Vid4 as the testing dataset.

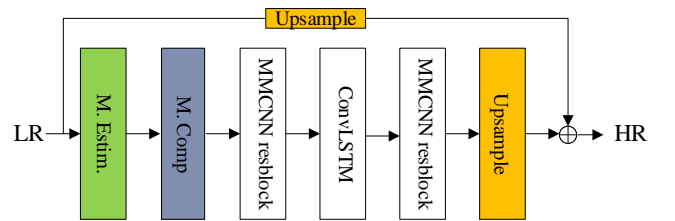


Fig. 14: The network architecture of MMCNN [18], where the MMCNN resblock denotes the multi-memory convolutional neural network with dense blocks.

11) *MMCNN*¹³: The architecture of the multi-memory convolutional neural network (MMCNN) [18] is shown in Fig. 14. MMCNN consists of 5 major modules including optical flow estimation, feature extraction, multi-memory detail fusion, feature reconstruction modules,

¹¹Code: <https://github.com/thunil/TecoGAN>

¹²Code: <https://github.com/anchen1011/toflow>

¹³Code: <https://github.com/psychopa4/MMCNN>

and a sub-pixel convolutional layer. Consecutive input frames are processed by the optical flow estimation module to make neighboring frames align with the target frame and then the warped frames are fed into subsequent network modules to attain the final super-resolution result of the target frame. In the multi-memory detail fusion module, MMCNN adopts the ConvLSTM [55] module to merge the spatio-temporal information. Moreover, the feature extraction, detail fusion, and feature reconstruction modules are all built based on residual dense blocks [41, 59], where the key difference of them only lies in the type of network layers.

For motion estimation and motion compensation, MMCNN adopts MCT in VESPCN [8]. The number of input frames is set to 5. The loss function consists of both the MSE and motion compensation loss. The *Myanmar*¹⁴ testing set, YUV21¹⁴, and Vid4 are used as the testing dataset.

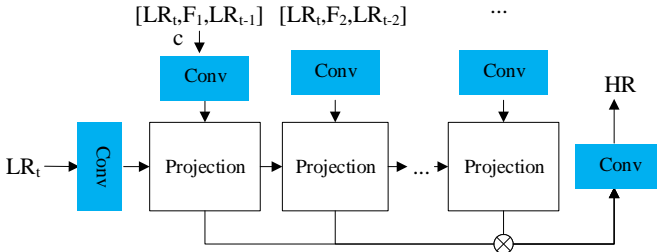


Fig. 15: The network architecture of RBPN [23], where \otimes denotes matrix multiplication.

12) *RBPN*¹⁵: Inspired by the back-projection algorithm [60, 61, 62], [23] proposed the recurrent back-projection network (RBPN), whose architecture is shown in Fig. 15. The network consists of a feature extraction module, one projection module, and one reconstruction module. The feature extraction module includes two operations, where one is to extract the features of the target frame, and another is to extract the feature from the concatenation of the target frame, the neighboring frame, and the calculated optical flow, which is from the neighboring frame to the target frame, and then perform alignment implicitly. The optical flow is obtained by pyflow¹⁶. The projection module consists of an encoder and a decoder. In the encoder, two feature maps which are output by the feature extraction module are conducted a single-image super-resolution and multi-image super-resolution, respectively. Then the subtraction image of the two yielded results is fed into the residual module to compute a residual. Finally, the sum of the residual and the super-resolution of the target frame is used as the output of the encoder, which is also the input of the decoder. In the decoder, the input is processed via both a residual module and a downsampling operation. The output of the decoder and the output of the feature

extraction module, which yields from the concatenation of the target frame, next neighboring frame and pre-computed optical flow, are used as the input to the next projection module. The above process does not stop until all neighboring frames are processed. That is, projection is used recurrently, which is the reason of the words “recurrent back-projection network”.

In RBPN, DBPN [62] is adopted as the single image super-resolution network, and ResNet [63] with deconvolution is used as the multi-image super-resolution network. RBPN uses the Vimeo-90K [22] dataset as the training set and testing set, and meanwhile uses data augmentation techniques. Batch size and patch size are set to 8 and 64×64 , respectively. The ℓ_1 -norm loss and Adam are used as the training loss function and optimizer, respectively. The initial learning rate is set to 10^{-4} , and it reduces to one tenth of the initial learning rate when performing half of total iterations.

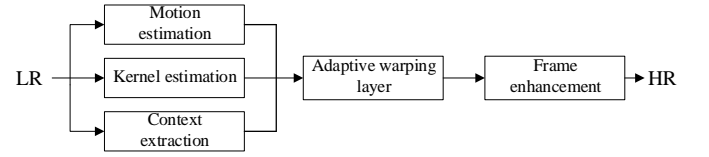


Fig. 16: The network architecture of MEMC-Net [19].

13) *MEMC-Net*¹⁷: The motion estimation and motion compensation network (MEMC-Net) [19], as shown in Fig. 16, proposes an adaptive warping layer. It warps the neighboring frame through the estimated optical flow and the convolutional kernel, which are resulted from a motion estimation network and a kernel estimation network, respectively, and aligns the neighboring frame with the target frame. The motion estimation network adopts FlowNet [45], and the kernel estimation network adopts an improved U-Net [57] including five max-pooling layers, five un-pooling layers and skip connections from the encoder to the decoder.

In MEMC-Net, the architecture of the super-resolution module is similar to that of EDSR [64]. In addition, in order to deal with the occlusion problem, it adopts a pre-trained ResNet18 [63] to extract the feature of input frames. Moreover, it feeds the output of the first convolutional layer of ResNet18 as the context information into the adaptive warping layer to perform the same warp operation. MEMC-Net adopts Vimeo-90K as the training set and testing set, the Charbonnier (Cb) function as the loss function, and Adam [54] as the optimizer for the network. The Cb function is defined as:

$$\mathcal{L} = \frac{1}{N} \sum_{i=1}^N \sqrt{\|\hat{I}_t^i - I_t^i\|_2^2 + \epsilon^2} \quad (12)$$

where $\|x\|_2$ denotes the ℓ_2 -norm ($\|x\|_2 = \sqrt{\sum_i x_i^2}$), N equals to the size of batch, and ϵ is set to 0.001.

¹⁴<http://www.codersvoice.com/a/webbase/video/08/152014/130.html>

¹⁵Code: <https://github.com/alterzero/RBPN-PyTorch>

¹⁶<https://github.com/pathak22/pyflow>

¹⁷Code: <https://github.com/baowenbo/MEMC-Net>

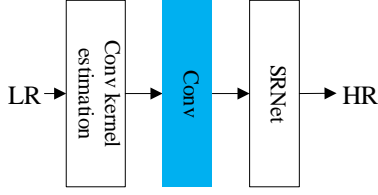


Fig. 17: The network architecture of RTVSR [21].

14) *RTVSR*: The real-time video super-resolution (RTVSR) [21], as shown in Fig. 17, adopts a convolutional network called motion convolutional kernel estimation network, which is a full convolution codec structure to estimate the motion between the target frame and the neighboring frame and produce a pair of 1D convolutional kernel corresponding to the current target frame and neighboring frame. Then the neighboring frame is warped by using estimated convolutional kernels to make it align with the target frame.

RTVSR first adopts the motion convolutional kernel network to perform the convolutional kernel estimation for the target frame and neighboring frame, and produces a pair of 1D convolutional kernels that represent the horizontal and vertical directions, respectively. Then the estimated convolutional kernels are used to warp the neighboring frame. Then the warped frame and target frame are fed into the subsequent super-resolution network to obtain the super-resolution result of the target frame. RTVSR designs an important component called gated enhance units (GEUs), which is an improved variant based on [65]. Its feature is that the output of residual blocks is not an element-wise addition between the input and output, but is a sum of the input and output with learned weights. RTVSR uses 261 videos with resolution of $3,840 \times 2,160$ from harmonicinc.com as the training set and adopts data augmentation to enlarge the training set. The GT videos are obtained by downsampling the original videos to the resolution of 960×540 . Vid4 is used as the testing set. RTVSR utilizes Adam as the optimizer and MSE as loss function. Patch size and batch size are set to 96×96 and 64, respectively.

15) *MultiBoot*: The multi-stage multi-reference bootstrapping method (called MultiBoot) [20] for video super-resolution consists of two stages. The output of the first stage is used as the input of the second stage in order to further improve performance. Its network architecture is shown in Fig. 18. The frames are input to the FlowNet 2.0 [48] to compute optical flow and perform the motion compensation operation. Then the processed frames are fed into the first-stage network to attain the super-resolution result of the target frame. In the second stage of MultiBoot, the output from the previous stage is downsampled, concatenated with the initial LR frame, and input to the network to obtain the final super-resolution result for the target frame.

It adopts REDS [66, 67] as the training set and testing set. Moreover, it also uses commonly used data augmen-

tation techniques. The Huber loss function \mathcal{H} is used for training, and is defined as:

$$\mathcal{H}(I_t - \tilde{I}_t) = \begin{cases} \frac{1}{2} \|I_t - \tilde{I}_t\|_2^2, & \|I_t - \tilde{I}_t\|_1 \leq \delta, \\ \delta \|I_t - \tilde{I}_t\|_1 - \frac{1}{2} \delta^2, & \text{otherwise} \end{cases} \quad (13)$$

where $\|x\|_1$ denotes the ℓ_1 -norm ($\|x\|_1 = \sum_i |x_i|$), I_t and \tilde{I}_t denote the HR image and the estimated HR image at time t . Note that $\delta = 1$, which is the point where the Huber loss function changes from a quadratic function to a linear one.

Motion estimation and motion compensation techniques are used to align neighboring frames with the target frame, which is the most common method for solving the video super-resolution problem. However, the problem is that they cannot guarantee the accuracy of motion estimation, which straightly affects the performance of video super-resolution. For this reason, the deformable convolution is proposed as one module in the deep network to align the frames. Its details are described in the following.

B. Deformable Convolution Methods

The deformable convolutional network was first proposed by Dai et al. [68] in 2017 and the improved version [69] was proposed in 2019. In ordinary convolutional neural networks, the convention is to use a fixed size for all the kernels in a layer, which restricts the network's capability to model geometric transformations. In contrast, the deformable convolution is able to relieve this limitation. The input feature maps are mapped to attain offsets via additional convolutional layers. The offsets are added to the conventional convolution kernel to yield a deformable convolution kernel, and then it is convolved with the input feature maps to produce the output feature maps. The illustration of the deformable convolution is shown in Fig. 19. Although deformable convolution increases the adaptability of the network to spatial deformation, the computational cost also increases. The methods that adopt deformable convolution mainly include the enhanced deformable video restoration (EDVR) [24], deformable non-local network (DNLN) [25], and temporally deformable alignment network (TDAN) [26], which are depicted in detail as follows.

1) *EDVR*¹⁸: The enhanced deformable video restoration (EDVR) method [24], as shown in Fig. 20, is the champion model in the NTIRE19 Challenge [66, 67]. EDVR proposes two key modules: the pyramid, cascading and deformable (PCD) alignment module [49, 70, 71, 72] and the temporal-spatial attention (TSA) fusion module, which are used to solve large motions in videos and to effectively fuse multiple frames, respectively.

EDVR consists of three parts, including one PCD alignment module, a TSA fusion module and a reconstruction module. Firstly, the input frames are aligned by the PCD

¹⁸Code: <https://github.com/xinntao/EDVR>

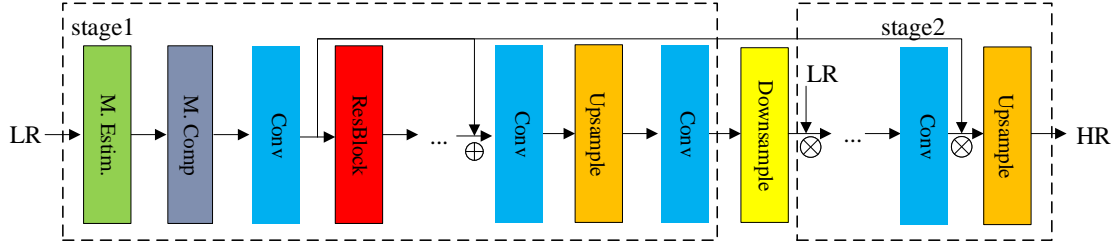


Fig. 18: The network architecture of MultiBoot [20].

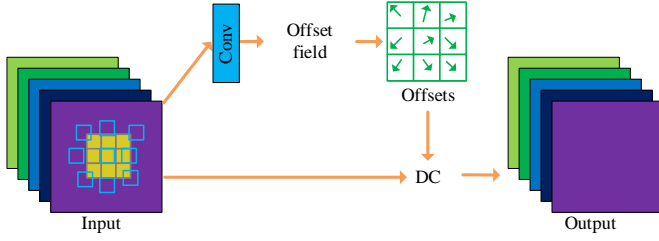


Fig. 19: A deformable convolution network.

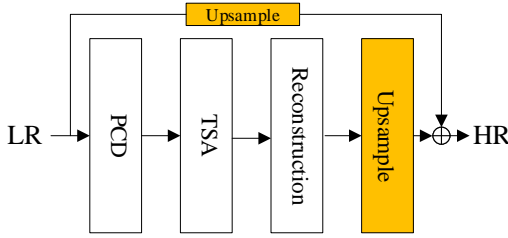


Fig. 20: The network architecture of EDVR [24], where PCD is the pyramid, cascading and deformable alignment module, and TSA is the temporal-spatial attention fusion module.

alignment module, and then the aligned frames are fused by the TSA fusion module. Then the fused results are fed into the reconstruction module to refine the features, and then through the up-sampling, a HR image called the residual image is obtained. The final result is obtained by adding the residual image to a direct upsampling target frame. To further improve performance, EDVR also adopts a two-phase approach, whose second phase is similar to the first phase but with a shallower network depth.

EDVR uses the realistic and dynamic scenes (REDS) dataset, which is proposed in the NTIRE19 Challenge, as the training set. The dataset is composed of 300 video sequences with resolution of $720 \times 1,280$, and each video has 100 frames, where the training set, the validation set and the testing set have 240, 30 and 30 videos, respectively. In the experiment, because the ground truth of the testing set can not be obtained, the authors regroup the rest of the videos. They select 4 representative videos (REDS4) as the testing set, and the rest of videos are used as the training set with data augmentation. In addition, EDVR adopts the Cb function as the loss

function and Adam as the optimizer, and it takes five consecutive frames as input. Patch size and batch size are set to 64×64 and 32, respectively. The initial learning rate is set to 4×10^{-4} .

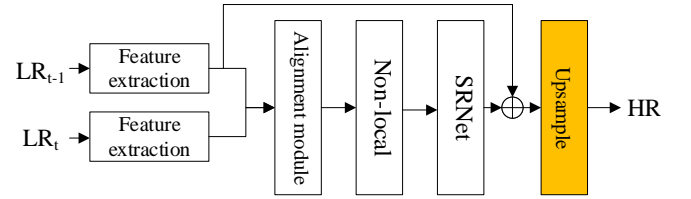


Fig. 21: The network architecture of DNLN [25].

2) *DNLN*¹⁹: The deformable non-local network (DNLN) [25], as shown in Fig. 21, designs an alignment module and a non-local attention module based on the deformable convolution [68, 69] and non-local networks [73]. The alignment module uses the hierarchical feature fusion module (HFFB) [74] within the original deformable convolution to generate convolutional parameters. Moreover, DNLN utilizes multiple deformable convolutions by a cascaded way, which makes inter-frame alignment more accurate. The non-local attention module takes the target frame and the aligned neighboring frames as input, and generates attention guided features by the non-local operation.

The whole network of DNLN consists of one feature extraction module, an alignment module, a non-local attention module and one reconstruction module, where the feature extraction module is composed of one convolutional layer and 5 residual blocks. The alignment module consists of 5 deformable convolutional layers, and the reconstruction module is made up of 16 residual in residual dense blocks (RRDB). The features of the target frame and the neighboring frame are first extracted by the feature extraction module, and then their features are fed into the alignment module to make the feature of the neighboring frame align with the feature of the target frame. The aligned features and target feature are fed into the non-local attention module to extract their correlations, and then the extracted correlations are fused by the reconstruction module. The output of the reconstruction module is added to the feature of the target frame, whose result is then up-sampled by

¹⁹Code: <https://github.com/wh1h/DNLN>

an upsampling layer to attain the final super-resolution result for the target frame.

DNLN adopts Vimeo-90K as the training set, and also uses data augmentation techniques. LR images are generated by downscaling the HR images with factor $\times 4$. Patch size is set to 50×50 . DNLN adopts the ℓ_1 -norm loss as the loss function and Adam as the optimizer.

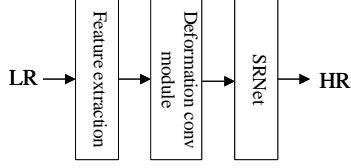


Fig. 22: The network architecture of TDAN [26].

3) *TDAN*²⁰: The temporally deformable alignment network (TDAN) [26], as shown in Fig. 22, applies deformable convolution to the target frame and the neighboring frame, and attains corresponding offsets. Then the neighboring frame is warped in terms of the offsets to align with the target frame.

TDAN can be divided into the two parts, i.e., an alignment module and a reconstruction module. In the alignment module, the target frame and the neighboring frame are taken as input. Then their features are separately extracted by a feature extraction layer consisting of convolutional layers and residual blocks, and then the obtained features are concatenated. The concatenated features are fed into a bottleneck layer to fuse features and reduce the number of channels. The output is then fed into an offset generator with deformable convolution to generate the corresponding offsets. Then the generated offset is used to conduct deformable convolution on the neighboring feature maps, and thus the aligned feature maps are obtained. The aligned feature maps are then processed by a convolutional layer to attain the aligned low-resolution frame. Moreover, the low-resolution frame concatenates with the target frame. Finally, the concatenated result is fed into the reconstruction module, which is a common super-resolution network, to output the super-resolution result for each target frame.

TDAN adopts Vimeo-90K as the training set, and uses the combination of the ℓ_1 -norm loss and motion compensation loss as the loss function, and Adam as the optimizer. The initial learning rate is set to 10^{-4} . Five consecutive frames are taken as input. Patch size and batch size are set to 48×48 and 64, respectively.

V. SPATIAL NON-ALIGNED METHODS

Different from the aligned methods, the non-aligned methods do not perform frame alignment before reconstruction. For the spatial non-aligned methods, instead of alignment operations such as motion estimation and motion compensation between frames, the input frames are

directly fed into a 2D convolutional network to spatially perform feature extraction, fusion and super-resolution operations. This may be an easier approach for solving the video super-resolution problem since it makes the network learn the correlation information within frames by itself. Next, we will introduce the related state-of-art methods in details.

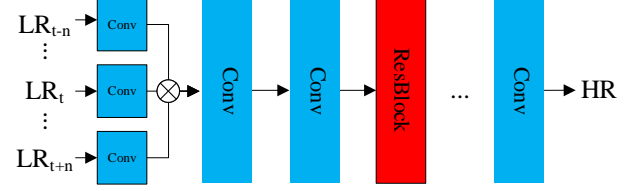


Fig. 23: The network architecture of VSRResNet [28].

1) *VSRResNet*: VSRResNet [28], as shown in Fig. 23, utilizes GAN to address video super-resolution and find a good solution by adversarial training. The generator consists of three 3×3 convolutional layers and residual blocks, where the residual block is composed of two 3×3 convolutional layers, each of which is followed by a ReLU activation function. The discriminator consists of three groups of convolutions, i.e., Batch Normalization (BN), LeakyReLU, and a fully connected layer.

The input frames of the generator are not aligned properly with multiple frames, but are up-sampled and fed directly into the network. It first conducts the 3×3 convolutional operation for each of multiple frames, and then the outputs are concatenated and perform feature fusion via a convolutional layer. The fused features are fed into multiple consecutive residual blocks, and finally the super-resolution result of the target frame is obtained by a 3×3 convolutional layer. The discriminator determines whether the output of the generator is a generated image or GT image. Then the result of the discriminator reacts to the generator, and promotes it to yield results closer to the GT images. Finally, a relative satisfactory solution is obtained through an iterative optimization.

For training the network, the generator is first trained, and then the generator and the discriminator are trained jointly. The loss function of VSRResNet consists of the adversarial loss, content loss, and perception loss, which is implemented by a VGG [75] to extract the features of the generated image and corresponding GT image, respectively, and then computing the loss using extracted features through the Cb loss function. The content loss denotes the Cb loss calculated between the generated result and GT.

Moreover, VSRResNet adopts the videos from *Myanmar*¹ as the training set, Vid4 as the testing set, and Adam as the optimizer. The number of input frames is set to 5 and the batch size is set to 64.

2) *FFCVSR*²¹: The architecture of the frame and feature-context video super-resolution (FFCVSR) method

²⁰Code: <https://github.com/YapengTian/TDAN-VSR-CVPR-2020>

²¹Code: <https://github.com/linchuming/FFCVSR>

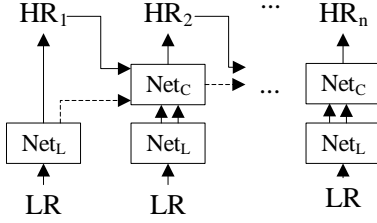


Fig. 24: The network architecture of FFCVSR [27].

[27] is illustrated in Fig. 24. Unlike normal motion estimation and motion compensation techniques, FFCVSR utilizes inter-frame information in a different way. In this work, the low-resolution unaligned video frames and the high-resolution output of the previous frame are directly taken as input to the network for the purpose of restoring high-frequency details and maintaining temporal consistency.

FFCVSR consists of a local network and a context network, where the local network consists of 5 convolutional layers, 1 deconvolution layer, and 8 residual blocks, each of which is composed of 2 convolutional layers and a skip connection. The local network is responsible for producing corresponding features and HR target frame based on the LR input frames. The context network consists of 5 convolutional layers, 1 deconvolution layer, 4 residual blocks, and 2 space-to-depth transformation layers.

Moreover, it has been found that simply inputting the previous recovered HR frames to the next context network leads to jitter and jagged artifacts. The solution is that for each sequence of T frames, the output of the current local network is used as the output of the previous context network. This method is called the suppression updating algorithm. The training set of FFCVSR comes from harmonicinc.com including Venice and Myanmar with resolution of 4K, and Vid4 is used as the testing set. FFCVSR adopts MSE as the loss function, Adam as the optimizer. The initial learning rate is set to 10^{-4} .

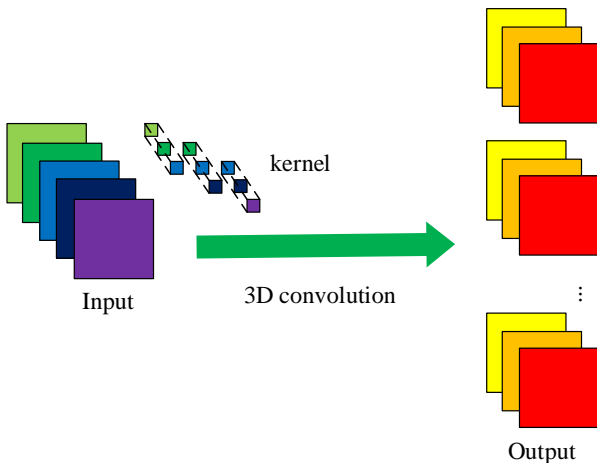


Fig. 25: The flowchart of 3D convolution.

VI. SPATIO-TEMPORAL NON-ALIGNED METHODS

Besides the spatial methods, another category of non-aligned methods are the spatio-temporal methods, whose characteristic is to exploit both the spatial and temporal information from input videos. According to utilizing of dominating techniques, spatio-temporal methods are classified into the following three classes: the 3D convolution (3D Conv), recurrent convolutional neural networks (RCNN) and non-local based methods. Next, we will introduce the related state-of-art methods in details.

A. 3D Convolution Methods

The 3D convolutional module [76, 77] can operate on the spatio-temporal domain, compared with the 2D convolution, which only utilizes the spatial information through the sliding kernel over the input frame. This is beneficial to the processing of video sequences, as the correlations among frames can be considered by extracting temporal information. The flowchart of 3D convolution is shown in Fig. 25. The representative 3D convolution methods include DUF [29], FSTRN [32], and 3DSRnet [31].

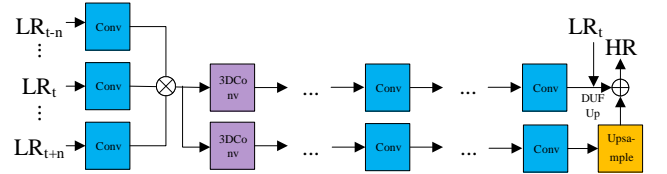


Fig. 26: The network architecture of DUF [29].

1) *DUF*²²: Inspired by the dynamic filter network [78] that can generate corresponding filters for specific inputs and then apply them to generate corresponding feature maps, the dynamic upsampling filters (DUF) method [29] has been proposed, as shown in Fig. 26. The structure of the dynamic up-sampling filter combined with spatio-temporal information learned by 3D convolution can avoid the use of motion estimation and motion compensation. DUF performs not only filtering, but also the up-sampling operation. In order to enhance high frequency details of the super-resolution result, DUF uses a network to estimate residual map for the target frame. The final result of one frame is the sum of the residual map and the frame processed by the dynamic up-sampling filter.

DUF also proposed a data augmentation method in the temporal axis for video data. By sampling frames in order or in reverse order at different time intervals, videos with different motion speed and directions can be obtained. In the experiment, DUF uses the Huber function as its loss function, where $\delta = 0.01$. Adam is used as the optimizer, and the initial learning rate is set to 10^{-3} .

²²Code: <https://github.com/yhjo09/VSR-DUF>

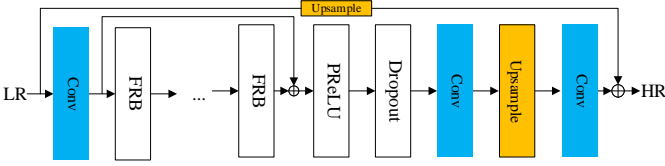


Fig. 27: The network architecture of FSTRN [32].

2) *FSTRN*: The fast spatio-temporal residual network (FSTRN) [32] method, as shown in Fig. 27, uses an adjusted 3D convolution to extract information among consecutive frames. In this method, a $k \times k \times k$ 3D convolutional kernel is decomposed into 2 cascaded kernels, whose sizes are $1 \times k \times k$ and $k \times 1 \times 1$, respectively, to reduce the amount of computation caused by directly using the 3D convolution.

FSTRN consists of the following four parts: one LR video shallow feature extraction net (LFENet), fast spatio-temporal residual blocks (FRBs), one LR feature fusion and up-sampling SR net (LSRNet), and a global residual learning (GRL) module. LFENet is composed of a C3D layer [76], which performs feature extraction for consecutive LR input frames. FRBs is composed of multiple FRB, each of which consists of a PReLU activation function and 2 decomposed 3D convolutional layers. It is responsible for extracting spatio-temporal information among input frames. LSRNet consists of 2 C3D layers and a deconvolution layer, and is in charge of fusing information from previous layers and conducting up-sampling. GRL is composed by both the LR space residual learning (LRL) and cross-space residual learning (CRL), where LRL is used at the beginning and the end of FRBs to improve the performance of feature extraction, and CRL is used for delivering the up-sampled LR input frame to the output of the whole network, and then both of them are added to obtain the final SR result. Besides, FSTRN adopts a dropout layer after LRL to enhance the generation ability of the network. In the experiment, FSTRN uses 25 video sequences with the *YUV* format⁴ as the training set, videos in [79] as the testing set (including Dancing, Flag, Fan, Treadmill and Turbine). The number of input frames is 5. The Cb function is used as the loss function, and Adam is used as the optimizer for training the network. The initial learning rate is set to 10^{-4} and the batch size is set to 144×144 .

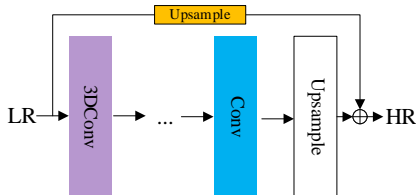


Fig. 28: The network architecture of 3DSRNet [31].

3) *3DSRnet*²³: The 3D super-resolution network (3DSRNet) [31] uses 3D convolution to extract spatio-temporal information among consecutive video frames for video super-resolution tasks. The network architecture is shown in Fig. 28. As the network goes deeper, the depth of feature maps after 3D convolution becomes shallower as well. In order to keep the depth and retain temporal information, 3DSRNet adopts an extrapolation operation, which adds one frame at the beginning and the end of the consecutive frames, respectively. Besides, 3DSRNet proposes an approach for scene change in practical applications, where a shallow classification network is proposed to judge input consecutive frames. If the scene change is detected in the current frame, it will be replaced by the frame that has the same scene and is the closest to the current frame. The substituted sequences will be sent to the subsequent video super-resolution network. This approach effectively solves the problem of performance degradation caused by scene change. In experimental settings, the kernel size of 3D convolutional is $3 \times 3 \times 3$. 3DSRNet uses MSE as its loss function, Adam as the optimizer, and Xavier as the method of weight initialization. The number of input frames is 5.

In brief, these 3D convolutional methods extract spatio-temporal correlations among consecutive frames, rather than perform the motion estimation to extract motion information among frames and motion compensation to align them. However, they have a large amount of computation.

B. Recurrent Convolutional Neural Networks

It is well known that RCNN have strong power of temporal dependency in modeling sequential data processing, e.g., natural language, video, audio, etc. A straightforward way is to use RCNN to handle video sequences. Based on this key idea, several RCNN methods such as STCN [33], BRCN [30], RISTN [35] and RRCN [34] have been proposed for video super-resolution.

1) *STCN*: The spatio-temporal convolutional network (STCN) [33], as shown in Fig. 29, is an end-to-end video super-resolution method without motion estimation and motion compensation. The temporal information within frames is extracted by using LSTM [80]. Similar to RISTN [35], the network consists of three parts: a spatial module, one temporal module and one reconstruction module.

Firstly, multiple consecutive up-sampled LR video frames are taken as input and then each frame is convoluted in the spatial module to extract features. Then the outputs are sent to the BMC-SLTM recurrent layer in the temporal module to extract temporal correlation. BMC-LSTM is a bidirectional multi-scale convolution version of LSTM. Finally, a convolution is performed to attain the HR result of the target frame. The spatial module is composed of 20 convolutional layers with

²³Code: <https://github.com/sooyekim/3DSRnet>

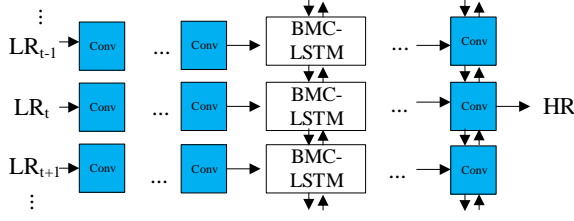


Fig. 29: The network architecture of STCN [33].

kernel size 3×3 , where the kernel number is 64. The temporal module consists of three layers, each of which consists of multiple BMC-LSTM submodules.

The input frame number of STCN is 5. Under this condition, the corresponding spatial module consists of 5 branches and each branch has 20 convolutional layers. The temporal module consists of 3 layers and each has five BMC-LSTM submodules. Then the reconstruction module consists of 1 convolutional layer. STCN adopts MSE as its loss function. In particular, the loss function calculates the difference between the reconstruction result of the adjacent frames and the corresponding HR frame, as well as the difference between the reconstruction result of the target frame and the corresponding HR frame. During training, the weight of the loss of the adjacent frame in its total loss is controlled by gradually decaying the balance parameter from 1 to 0. Besides, STCN uses Adam as the optimizer with batch size 64, and initial learning rate is 10^{-4} .

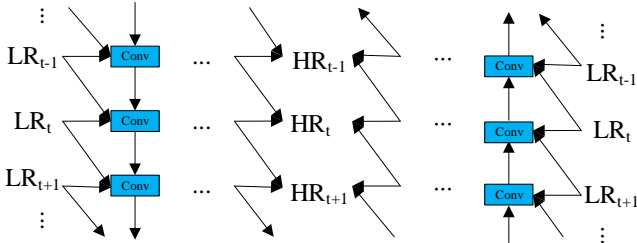


Fig. 30: The network architecture of BRCN [30].

2) *BRCN*: The bidirectional recurrent convolutional network (BRCN) [30], as shown in Fig. 30, utilizes the unique advantage of RCNN that is suitable for processing sequence data, to deal with the dependence among consecutive frames in a video.

BRCN is composed of two modules including a forward sub-network and a backward one with a similar structure, which only differ in the order of processing sequence. Here we define $X_{i=1,2,\dots,T}$ as a set of low-resolution video frames interpolated by a general bicubic method. In the forward subnet, the input of each node in the hidden layer comes from three parts: the output of the previous layer at the current time i , and at time $i-1$, and the output of the previous node in the current layer, respectively. Note that these 3 outputs are all resulted from the corresponding convolutional operation, which are named as feedforward convolution, condi-

tional convolution and recurrent convolution, respectively. The feedforward convolution is used to extract spatial dependence, while the other two convolutions are used to extract temporal dependence among consecutive frames. Finally, the output of the whole network is the combination of the output from the two sub-networks as follows: The output of the feedforward convolution at the current time and the output from the conditional convolution at time $i-1$ in the forward sub-network. The output of the feedforward convolution at the current time and the output from the conditional convolution at time $i+1$ in the backward sub-network.

BRCN uses 25 video sequences in the YUV format as the training set, the video sequences in [79] as the testing set. The patch size is 32×32 , the the number of input frames is 10, and MSE is as its loss function. The network is optimized through stochastic gradient descent (SGD).

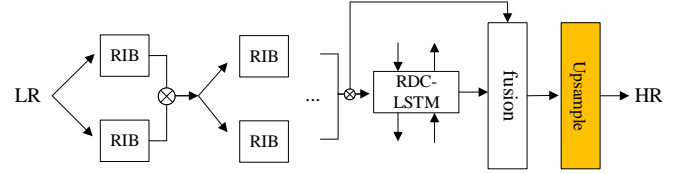


Fig. 31: The network architecture of RISTN [35].

3) *RISTN*²⁴: The residual invertible spatio-temporal network (RISTN) [35] is shown in Fig. 31. It is inspired by the invertible block [81] and designs a residual invertible block (RIB), which is used to extract spatial information of video frames effectively, a LSTM with residual dense convolution, which is used to extract spatio-temporal features, and a sparse feature fusion strategy to adaptively select useful features.

The network is divided into three parts: one temporal module, a spatial module and one reconstruction module. The spatial module is mainly composed of multiple parallel RIBs, and its output is used as the input of the temporal module. In the temporal module, after extracting spatio-temporal information, features are selectively fused by a sparse fusion strategy. Finally, the HR result of the target frame is reconstructed by the deconvolution in the reconstruction module. In the experiment in [35], RISTN randomly selects 50K images from the ImageNet dataset to pre-train the spatial module and then uses 192 videos with resolution $1,920 \times 1,080$ collected from 699pic.com and vimeo.com as the training set to train the whole network. RISTN uses the mean MSE as its loss function, and the sparse matrix is constrained by the ℓ_1 -norm regularization term. Besides, the number of input frames is set to 5. The super-resolution scale is 4, and Vid4 is used as the testing set.

4) *RRCN*: The residual recurrent convolutional network (RRCN) [34], as shown in Fig. 32, is a bidirectional recurrent neural network, which learns a residual image. RRCN proposes an unsynchronized full recurrent

²⁴Code: <https://github.com/lizhuangzi/RISTN>

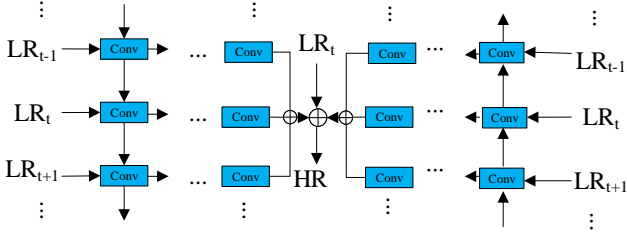


Fig. 32: The network architecture of RRCN [34].

convolutional network, where unsynchronization refers to the input of multiple consecutive video frames, and only the middle one is super-resolved.

RRCN uses the combined local-global with total variable (GLG-TV) method [47] to perform motion estimation and compensation for the target frame and its adjacent frames. The compensated frames are used as input to the network. The forward and recurrent convolutions are conducted in the forward network and the backward network, respectively, and their outputs are summed up. Finally, the result is obtained by adding the target frame in the input. In order to further improve the performance, RRCN also uses the self-ensemble strategy and combines it with the output of the single image super-resolution method, EDSR+ [64], to obtain two models named RRCN+ and RRCN++, respectively.

The proposed RRCN method consists of 15 convolutional layers. Except the last layer, the forward convolution in other layers uses the 3×3 convolutional kernel and 32 feature maps. In the last layer, though it uses the 3×3 convolutional kernel, the number of feature maps depends on the final output format. The recurrent convolution is with 1×1 kernel and 32 feature maps. Moreover, RRCN uses the Myanmar video as the training set, and uses Myanmar (except for training data), Vid4, and YUV21 as the testing set. MSE is used as the loss function, and RMSProp is used as the optimization method. The number of input frames is 5, and the patch size is 81×81 . The up-sampled and compensated LR frames are used as the input for RRCN.

C. Non-Local Methods

The non-local-based method is another one that utilizes both the spatial and temporal information in video frames for super-resolution. This method benefit from the key idea of the non-local neural network [73], which was proposed to capture long-range dependencies for video classifications. It overcomes the flaws that convolution and recurrent computations are limited to the local area. A non-local operation, intuitively, is to calculate the response value of a position, which is equal to the weight sum of all possible positions in the input feature maps. Its formula is given as follows:

$$y_i = \frac{1}{\mathcal{C}(x)} \sum_{\forall j} f(x_i, x_j) g(x_j) \quad (14)$$

where i is the index of the output location where the response value needs to be calculated, j is the index of all possible locations, x and y are the input and output data with the same dimensions, respectively, f is a function to calculate the correlation between i and j , g is the function which calculates the feature representation of input data and $\mathcal{C}(x)$ is the normalization factor. Here, g is usually defined as: $g(x_j) = W_g x_j$, where W_g is the weight matrix that needs to learn. f has multiple choices such as Gaussian, embedded Gaussian, dot product, and concatenation.

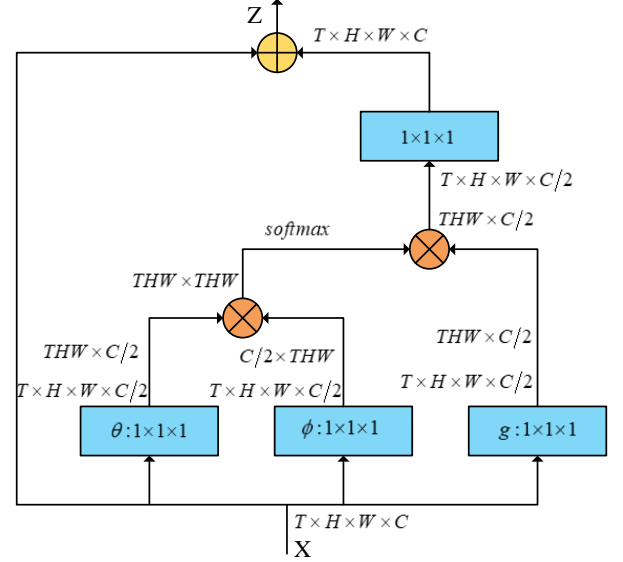


Fig. 33: The details of a non-local block, where $T \times H \times W \times C$ denotes the size of feature maps, $\theta(\cdot)$, $\phi(\cdot)$ and $g(\cdot)$ are all linear embedding functions (see [73] for details).

A corresponding convolutional computation built from the above process is shown in Fig. 33. It is a spatio-temporal non-local block, where f is an embedded Gaussian function as follows:

$$f(x_i, x_j) = e^{\theta(x_i)^T \phi(x_j)} \quad (15)$$

where $\theta(x_i) = W_\theta x_i$, $\phi(x_j) = W_\phi x_j$, and $\mathcal{C}(x) = \sum_{\forall j} f(x_i, x_j)$.

The non-local block can easily be added into existing deep convolutional neural networks. Although non-local networks are able to capture spatio-temporal information effectively, the shortage, which is similar to 3D convolution, is that it has a large amount of computation.

One typical method based on non-local blocks is the progressive fusion non-local (PFNL) [36] method, as illustrated in Fig. 34. PFNL uses non-local residual blocks to extract spatio-temporal features, and the proposed progressive fusion residual block (PFRB) to fuse them. Finally, the output through a sub-pixel convolutional layer is added to the input frame that is up-sampled by the bicubic interpolation, which is the final super-resolution result. PFRB is composed of three convolutional layers. Firstly, the input frames are convoluted

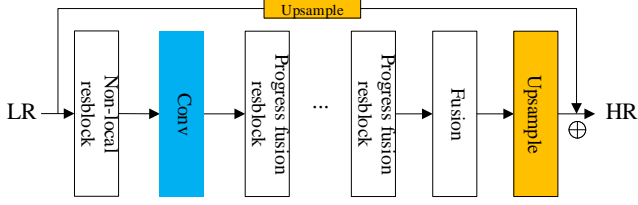


Fig. 34: The network architecture of PFNL [36].

by the 3×3 kernels, respectively, then the output feature maps are concatenated, and the channel dimension is reduced by performing the 1×1 convolution. And the results are concatenated with the previous convoluted feature maps, respectively, and conducted with a 3×3 convolution. The final results are added to each input frame to obtain the output for current PFRB. In addition, in order to avoid the increase of parameters brought by the superposition of PFRB, PFNL adopts the mechanism of parameter sharing between channels (refer to [82, 83]), which effectively balances trade-off between the number of parameters and network performance. PFNL chooses the Cb function as its loss function, and uses Adam as the optimizer and 10^{-3} as its initial learning rate.

VII. PERFORMANCE COMPARISON

In this section, we summarize the performance of the representative video super-resolution methods in Table IV in terms of both PSNR and SSIM. In the comparison, the magnification factors include 2, 3 and 4. The degradation types are the bicubic downsampling with the image-resize function (BI) and Gaussian blurring and downsampling (BD). Details of some widely used datasets in Table IV are listed in Table II. It's noted that some of the most popular datasets are summarized here.

Besides, we also summarize several international video super-resolution competitions in Table III. We believe that such competitions are giving great contributions to the development of video super-resolution and helping develop new methods for various video super-resolution applications. Therefore, they are worthy of more attention.

VIII. TREND AND CHALLENGE

Although great progress has been made by the state-of-the-art video super-resolution methods based on deep learning especially on some public benchmark datasets, there are still several challenges discussed below.

A. Lightweight Super-resolution Models

The deep learning based video super-resolution methods though enjoy high performance, they have difficulty in deploying efficiently in the real-world problems, because their models usually have a mass of parameters and require vast computing and storage resources, and their training takes a long time. With the popularity of

mobile devices in modern life, one expects to apply these models on such devices. How to design and implement a super-resolution algorithm that is high performance and lightweight for real-world applicants is one of the challenges.

B. Interpretability of Models

Deep neural networks are usually considered black boxes. That is, we are not able to know what real information the model learns when the performance is well or bad. In existing video super-resolution models, there is not a theoretical interpretation about how convolution neural networks recover low-resolution video sequences. With a deeper investigation in its interpretation, the performance of super-resolution algorithms including video and image super-resolution methods may be improved greatly.

C. Large Scale Super-resolution

For video super-resolution tasks, existing works mainly focus on the case of the magnification factor 4. The more challenging scales, such as $\times 8$, and $\times 16$, have been rarely explored. With the popularity of high resolution (e.g., 4K, 8K and 16K) display devices, larger scale super-resolution is to be further studied. Obviously, as the scale becomes larger, it is more challenging to predict and restore unknown information in video sequences. This may result in performance degradation for the algorithms, and weakened robustness in the models. Therefore, how to develop stable deep learning algorithms for larger scale video super-resolution is still an important issue.

D. More Reasonable and Proper Degradation Process of Video Quality

In existing works, the degraded LR videos is attained through two methods. One is directly downsampling HR videos by using interpolation, such as bicubic. Another is performing the Gaussian blurring on HR videos and then downsampling the video sequences. Although both methods perform well in theory, they always perform poorly in practice. As it is known, the real-world degradation process is very complex and includes much uncertainty in real-world problems, the blurring and interpolation is not inadequate for modeling the problem. Therefore, when constructing LR videos, the degradation should be modeled theoretically in consistent with the real-world case to reduce the gap between research and practice.

E. Unsupervised Super-resolution Methods

Most state-of-the-art video super-resolution methods are supervised learning. The deep neural networks require a large amount of paired LR and HR video frames for training. However, such paired datasets are rare

TABLE II: Some widely-used video super-resolution datasets. Note that ‘-’ represents unknown information.

Dataset	Year	Type	Download Link	Video Number	Resolution	Color Space
V-train1	-	Train	https://media.xiph.org/video/derf/	25	-	YUV
V-test	-	Test	https://media.xiph.org/video/derf/	5	-	YUV
Vid4	2011	Test	https://drive.google.com/drive/folders/10-gUO6zBeOpWEamrWKCTskkUFukB9W5m	4	720 × 480	RGB
YUV21	2014	Test	http://www.codersvoice.com/a/webbase/video/08/152014/130.html	21	352 × 288	YUV
Venice	2014	Train	https://www.harmonicinc.com/free-4k-demo-footage/	1	3,840 × 2,160	RGB
Myanmar	2014	Train	https://www.harmonicinc.com/insights/blog/4k-in-context/	1	3,840 × 2,160	RGB
CDVL	2016	Train	http://www.cdv1.org/	-	1,920 × 1,080	RGB
Vimeo90K	2019	Train+Test	http://toflow.csail.mit.edu/	91,701	448 × 256	RGB
REDS	2019	Train+Test	https://seungjunna.github.io/Datasets/reds.html	270	1,920 × 1,080	RGB
UVG	2020	Test	http://ultravideo.cs.tut.fi/	16	3,840 × 2,160	YUV

TABLE III: Some major video super-resolution competitions. Note that ‘EDVR+’ stands for a method based on EDVR, and ‘-’ represents unknown information.

Name	Year	Organizer	Location	Website	Dataset	Scale	Champion	PSNR	SSIM
NTIRE 2019 Video Restoration and Enhancement Challenges	2019	CVPR	Long Beach, California	https://data.vision.ee.ethz.ch/cvl/ntire19/	REDS	×4	EDVR [24]	31.79	0.8962
YOUKU Video Super-Resolution and Enhancement Challenge	2019	Alibaba	Hangzhou, China	https://tianchi.aliyun.com/competition/entrance/231711/introduction	Youku-VESR	×4	VESR-Net [84]	37.85	-
AIM 2019 Challenge on Video Extreme Super-Resolution	2019	ECCV	Hong Kong, China	https://www.aim2019.org/	Vid3oC	×16	EDVR+	22.53	0.64
Mobile Video Restoration Challenge	2019	ICIP & Kwai	-	https://www.kuaishou.com/activity/icip2019	-	-	-	-	-
AIM 2020 Challenge on Video Extreme Super-Resolution	2020	ECCV	Boston, Massachusetts	http://aim2020.org/	-	×16	-	-	-

or costly to obtained in practice. One may synthesize the LR/HR video frames, the performance of super-resolution methods is still not satisfied as the degradation model is too simple to characterize the real-world problem and results in inaccurate HR/LR datasets.

F. More Effective Scene Change Algorithms

Existing video super-resolution methods rarely involve the videos with scene change. In practice, a video sequence usually has many different scenes. When we consider the problem of video super-resolution on such videos, they have to be split into multiple segments without scene change and process individually. This may result in large computational time. Therefore, deep learning methods that can process videos with scene change are necessary for real-world applications.

G. More Reasonable Evaluation Criteria for Video Quality

The criterion for evaluating the quality of super-resolution results mainly includes PSNR and SSIM. However, their values are not able to reflect the video quality for human perception. That is, even if the PSNR value of a video is very high, the video is uncomfortable for human. Therefore, new video evaluation criteria that are consistent with human perception need to be developed. Some evaluation criteria have been proposed, nevertheless, more criteria which can be broadly accepted are still under in need.

H. More Effective Methods for Leveraging Information between Frames

An important characteristic of video super resolution is leveraging the information between frames. Utilizing it effectively influences the performance directly. Although, many methods have been proposed as mentioned in this work, there are still some disadvantages.

TABLE IV: Comparison of all the methods on the datasets with magnification factors 2, 3, and 4. Noted that 'Internet' means that the dataset is collected from the internet. '*' denotes that the source of the dataset is unknown, and '-' indicates that the method does not be tested on the datasets.

Method	TrainSet	TestSet	Scale	BI		BD	
				PSNR	SSIM	PSNR	SSIM
VSRnet [12]	Myanmar	Vid4	×2	31.30	0.9278	-	-
		Myanmar-T		38.48	0.9679	-	-
3DSRnet [31]	largeSet	Vid4		32.25	0.9410	-	-
		Vid4		33.50	0.9491	-	-
MMCNN [18]	*	Myanmar-T		39.37	0.9740	-	-
		YUV21		34.96	0.9371	-	-
DRVSR [14]	*	SPMCS		36.71	0.9600	-	-
VSRResNet [28]	Myanmar	Vid4		31.87	0.9426	-	-
BRCN [30]	V-trian	Vid4		-	-	28.77	0.8499
		V-test		-	-	32.84	0.8968
		Myanmar-T		40.47	0.9800	-	-
RRCN [34]	Myanmar	Vid4		33.41	0.9490	-	-
		YUV21		35.62	0.9425	-	-
DUF [29]	Internet	Vid4		-	-	33.73	0.9554
STCN [33]	*	Hollywood2		-	-	41.51	0.9804
VSRnet [12]	Myanmar	Vid4	×3	26.79	0.8098	-	-
		Myanmar-T		34.42	0.9247	-	-
VESPCN [8]	CDVL	Vid4		27.25	0.8447	-	-
3DSRnet [31]	largeSet	Vid4		27.70	0.8498	-	-
		Vid4		28.40	0.8722	-	-
MMCNN [18]	*	Myanmar-T		35.42	0.9393	-	-
		YUV21		30.82	0.8567	-	-
DRVSR [14]	*	Vid4		27.49	0.8400	-	-
		SPMCS		31.92	0.9000	-	-
VSRResNet [28]	Myanmar	Vid4		27.80	0.8571	-	-
		Myanmar-T		35.53	0.9446	-	-
RRCN [34]	Myanmar	Vid4		28.25	0.8618	-	-
		YUV21		31.35	0.8668	-	-
DUF [29]	Internet	Vid4		-	-	28.90	0.8898
STCN [33]	*	Hollywood2		-	-	37.03	0.9546
VSRnet [12]	Myanmar	Vid4	×4	24.84	0.7049	-	-
		Myanmar-T		31.85	0.8834	-	-
VESPCN [8]	CDVL	Vid4		25.35	0.7557	-	-
3DSRnet [31]	largeSet	Vid4		25.71	0.7588	-	-
		Vid4		26.28	0.7844	-	-
MMCNN [18]	*	Myanmar-T		33.06	0.9040	-	-
		YUV21		28.90	0.7983	-	-
		Vid4+tp+pg		28.97	-	-	-
TOFlow [22]	V-90K	Vid4		-	-	23.54	0.8070
		V-90K-T		-	-	33.08	0.9417
TecoGAN [10]	*	ToS		-	-	32.75	-
		Vid4		-	-	25.89	-
MultiBoot [20]	REDS	REDS-Test		31.00	0.8822	-	-
Deep-DE [11]	*	city+tp+pg		-	-	29.00	0.8870
SOFVSR [17]	CDVL	DAVIS-10		34.32	0.9250	-	-
		Vid4		26.01	0.7710	-	-
MEMC-Net [19]	V-90K	V-90K-T		33.47	0.9470	-	-
		Vid4		24.37	0.8380	-	-
FRVSR [16]	vimeo.com	Vid4		-	-	26.69	0.8220
RBPV [23]	V-90K	Vid4		27.16	0.8190	-	-
		SPMCS		30.10	0.8740	-	-
DRVSR [14]	*	Vid4		25.52	0.7600	-	-
		SPMCS		29.69	0.8400	-	-
FFCVSR [27]	Venice+Myanmar	Vid4		26.97	0.8300	-	-
VSRResNet [28]	Myanmar	Vid4		25.51	0.7530	-	-
		Vid4		27.35	0.8264	-	-
EDVR [24]	V-90K	V-90K-T		37.61	0.9489	-	-
	REDS	REDS4		31.09	0.8800	28.88	0.8361
TDAN [26]	V-90K	Vid4		26.24	0.7800	26.58	0.801
DNLN [25]	V-90K	Vid4		-	-	27.31	0.8257
		SPMCS		-	-	30.36	0.8794
RVSr [13]	V-train1	Vid4+tp+pg		28.05	-	-	-
		UVGD		39.71	-	-	-
FSTRN [32]	V-train	V-test		-	-	29.95	0.8700
		Vid4		-	-	24.43	0.6334
BRCN [30]	V-trian	V-test		-	-	28.20	0.7739
		Myanmar-T		32.35	0.9023	-	-
RRCN [34]	Myanmar	Vid4		25.86	0.7591	-	-
		YUV21		29.08	0.7986	-	-
DUF [29]	Internet	Vid4		-	-	26.81	0.8145
PFNL [36]	*	Vid4		-	-	27.40	0.8384
STCN [33]	*	Hollywood2		-	-	34.58	0.9259
		city+pg+tp		-	-	30.27	0.9103

For instance, 3D convolution and non-local modules have a large amount of computation, and the accuracy of optical estimation can not be guaranteed. Therefore, the methods that can effectively utilize information between frames is worth further studying.

IX. CONCLUSIONS

In this paper, we reviewed the development of deep learning for video super-resolution in recent years. Firstly, we classify existing video super-resolution algorithms by the way of leveraging information within frames. Then we found that though video super-resolution algorithms based on deep learning have made great progress, there are still some potential and unsolved problems. We summarized eight aspects, as mentioned above. The development of deep learning has entered its challenging period. As researchers further explore it, we believe that the above problems can be further addressed.

ACKNOWLEDGMENT

We thank all the reviewers for their valuable comments. This work was supported by the National Natural Science Foundation of China (Nos. 61876220, 61876221, 61976164, 61836009 and U1701267), the Project supported the Foundation for Innovative Research Groups of the National Natural Science Foundation of China (No. 61621005), the Program for Cheung Kong Scholars and Innovative Research Team in University (No. IRT_15R53), the Fund for Foreign Scholars in University Research and Teaching Programs (the 111 Project) (No. B07048), the Science Foundation of Xidian University (Nos. 10251180018 and 10251180019), the National Science Basic Research Plan in Shaanxi Province of China (Nos. 2019JQ-657 and 2020JM-194), and the Key Special Project of China High Resolution Earth Observation System-Young Scholar Innovation Fund.

REFERENCES

- [1] C. Liu and D. Sun, "On Bayesian adaptive video super resolution," *IEEE Transactions on Pattern Analysis and Machine Intelligence*, vol. 36, no. 2, pp. 346–360, 2013.
- [2] Z. Ma, R. Liao, X. Tao, L. Xu, J. Jia, and E. Wu, "Handling motion blur in multi-frame super-resolution," in *Proceedings of the IEEE Conference on Computer Vision and Pattern Recognition*, 2015, pp. 5224–5232.
- [3] Z. Wang, J. Chen, and S. C. Hoi, "Deep learning for image super-resolution: A survey," *IEEE Transactions on Pattern Analysis and Machine Intelligence*, 2020.
- [4] A. Singh and J. Singh, "Survey on single image based super-resolution-implementation challenges and solutions," *Multimedia Tools and Applications*, vol. 79, no. 3, pp. 1641–1672, 2020.
- [5] W. Yang, X. Zhang, Y. Tian, W. Wang, J.-H. Xue, and Q. Liao, "Deep learning for single image super-resolution: A brief review," *IEEE Transactions on Multimedia*, vol. 21, no. 12, pp. 3106–3121, 2019.
- [6] M. V. Daithankar and S. D. Ruikar, "Video super resolution: A review," in *ICDSMLA 2019, 2020*, pp. 488–495.
- [7] K. Seshadrinathan and A. C. Bovik, "Motion tuned spatio-temporal quality assessment of natural videos," *IEEE Transactions on Image Processing*, vol. 19, no. 2, pp. 335–350, 2010.
- [8] J. Caballero, C. Ledig, A. Aitken, A. Acosta, J. Totz, Z. Wang, and W. Shi, "Real-time video super-resolution with spatio-temporal networks and motion compensation," in *2017 IEEE Conference on Computer Vision and Pattern Recognition (CVPR)*, 2017, pp. 2848–2857.
- [9] R. Zhang, P. Isola, A. A. Efros, E. Shechtman, and O. Wang, "The unreasonable effectiveness of deep features as a perceptual metric," in *2018 IEEE Conference on Computer Vision and Pattern Recognition*, 2018, pp. 586–595.
- [10] M. Chu, Y. Xie, J. Mayer, L. Leal-Taixé, and N. Thuerey, "Learning Temporal Coherence via Self-Supervision for GAN-based Video Generation," *arXiv e-prints*, 2018.
- [11] R. Liao, X. Tao, R. Li, Z. Ma, and J. Jia, "Video super-resolution via deep draft-ensemble learning," in *2015 IEEE International Conference on Computer Vision (ICCV)*, 2015, pp. 531–539.
- [12] A. Kappeler, S. Yoo, Q. Dai, and A. K. Katsaggelos, "Video super-resolution with convolutional neural networks," *IEEE Transactions on Computational Imaging*, vol. 2, no. 2, pp. 109–122, June 2016.
- [13] D. Liu, Z. Wang, Y. Fan, X. Liu, Z. Wang, S. Chang, and T. Huang, "Robust video super-resolution with learned temporal dynamics," in *2017 IEEE International Conference on Computer Vision (ICCV)*, 2017, pp. 2526–2534.
- [14] X. Tao, H. Gao, R. Liao, J. Wang, and J. Jia, "Detail-revealing deep video super-resolution," in *2017 IEEE International Conference on Computer Vision (ICCV)*, 2017, pp. 4482–4490.
- [15] T. H. Kim, M. S. M. Sajjadi, M. Hirsch, and B. Schölkopf, "Spatio-temporal transformer network for video restoration," in *Computer Vision – ECCV 2018*, 2018, pp. 111–127.
- [16] M. S. M. Sajjadi, R. Vemulapalli, and M. Brown, "Frame-recurrent video super-resolution," in *2018 IEEE Conference on Computer Vision and Pattern Recognition*, 2018, pp. 6626–6634.
- [17] L. Wang, Y. Guo, Z. Lin, X. Deng, and W. An, "Learning for video super-resolution through HR optical flow estimation," in *Computer Vision – ACCV 2018, 2019*, pp. 514–529.
- [18] Z. Wang, P. Yi, K. Jiang, J. Jiang, Z. Han, T. Lu, and J. Ma, "Multi-memory convolutional neural network for video super-resolution," *IEEE Transactions*

- on *Image Processing*, vol. 28, no. 5, pp. 2530–2544, May 2019.
- [19] W. Bao, W. Lai, X. Zhang, Z. Gao, and M. Yang, “MEMC-Net: Motion estimation and motion compensation driven neural network for video interpolation and enhancement,” *IEEE Transactions on Pattern Analysis and Machine Intelligence*, 2019.
- [20] R. Kalarot and F. Porikli, “MultiBoot VSR: Multi-stage multi-reference bootstrapping for video super-resolution,” in *2019 IEEE Conference on Computer Vision and Pattern Recognition Workshops (CVPRW)*, 2019, pp. 2060–2069.
- [21] B. Bare, B. Yan, C. Ma, and K. Li, “Real-time video super-resolution via motion convolution kernel estimation,” *Neurocomputing*, vol. 367, pp. 236–245, 2019.
- [22] T. Xue, B. Chen, J. Wu, D. Wei, and W. T. Freeman, “Video enhancement with task-oriented flow,” *International Journal of Computer Vision*, vol. 127, no. 8, pp. 1106–1125, Aug 2019.
- [23] M. Haris, G. Shakhnarovich, and N. Ukita, “Recurrent back-projection network for video super-resolution,” in *2019 IEEE Conference on Computer Vision and Pattern Recognition (CVPR)*, 2019, pp. 3892–3901.
- [24] X. Wang, K. C. K. Chan, K. Yu, C. Dong, and C. C. Loy, “EDVR: Video restoration with enhanced deformable convolutional networks,” in *2019 IEEE Conference on Computer Vision and Pattern Recognition Workshops (CVPRW)*, 2019, pp. 1954–1963.
- [25] H. Wang, D. Su, C. Liu, L. Jin, X. Sun, and X. Peng, “Deformable non-local network for video super-resolution,” *IEEE Access*, vol. 7, pp. 177 734–177 744, 2019.
- [26] Y. Tian, Y. Zhang, Y. Fu, and C. Xu, “TDAN: Temporally-deformable alignment network for video super-resolution,” in *Proceedings of the IEEE Conference on Computer Vision and Pattern Recognition*, 2020, pp. 3360–3369.
- [27] B. Yan, C. Lin, and W. Tan, “Frame and feature-context video super-resolution,” in *The Thirty-Third AAAI Conference on Artificial Intelligence*, 2019, pp. 5597–5604.
- [28] A. Lucas, S. LApez-Tapia, R. Molina, and A. K. Katsaggelos, “Generative adversarial networks and perceptual losses for video super-resolution,” *IEEE Transactions on Image Processing*, vol. 28, no. 7, pp. 3312–3327, July 2019.
- [29] Y. Jo, S. W. Oh, J. Kang, and S. J. Kim, “Deep video super-resolution network using dynamic upsampling filters without explicit motion compensation,” in *2018 IEEE Conference on Computer Vision and Pattern Recognition*, 2018, pp. 3224–3232.
- [30] Y. Huang, W. Wang, and L. Wang, “Video super-resolution via bidirectional recurrent convolutional networks,” *IEEE Transactions on Pattern Analysis and Machine Intelligence*, vol. 40, no. 4, pp. 1015–1028, April 2018.
- [31] S. Y. Kim, J. Lim, T. Na, and M. Kim, “Video super-resolution based on 3d-cnns with consideration of scene change,” in *2019 IEEE International Conference on Image Processing (ICIP)*, 2019, pp. 2831–2835.
- [32] S. Li, F. He, B. Du, L. Zhang, Y. Xu, and D. Tao, “Fast spatio-temporal residual network for video super-resolution,” in *Proceedings of the IEEE Conference on Computer Vision and Pattern Recognition*, 2019, pp. 10 522–10 531.
- [33] J. Guo and H. Chao, “Building an end-to-end spatial-temporal convolutional network for video super-resolution,” in *Proceedings of the Thirty-First AAAI Conference on Artificial Intelligence*, 2017, pp. 4053–4060.
- [34] D. Li, Y. Liu, and Z. Wang, “Video super-resolution using non-simultaneous fully recurrent convolutional network,” *IEEE Transactions on Image Processing*, vol. 28, no. 3, pp. 1342–1355, March 2019.
- [35] X. Zhu, Z. Li, X. Zhang, C. Li, Y. Liu, and Z. Xue, “Residual invertible spatio-temporal network for video super-resolution,” in *The Thirty-Third AAAI Conference on Artificial Intelligence (AAAI)*, 2019, pp. 5981–5988.
- [36] P. Yi, Z. Wang, K. Jiang, J. Jiang, and J. Ma, “Progressive fusion video super-resolution network via exploiting non-local spatio-temporal correlations,” in *2019 IEEE International Conference on Computer Vision (ICCV)*, 2019, pp. 3106–3115.
- [37] C. Dong, C. C. Loy, K. He, and X. Tang, “Learning a deep convolutional network for image super-resolution,” in *Computer Vision – ECCV 2014*, 2014, pp. 184–199.
- [38] C. Dong, C. C. Loy, and X. Tang, “Accelerating the super-resolution convolutional neural network,” in *Computer Vision – ECCV 2016*, 2016, pp. 391–407.
- [39] J. Kim, J. K. Lee, and K. M. Lee, “Accurate image super-resolution using very deep convolutional networks,” in *2016 IEEE Conference on Computer Vision and Pattern Recognition (CVPR)*, 2016, pp. 1646–1654.
- [40] W. Shi, J. Caballero, F. Huszar, J. Totz, A. P. Aitken, R. Bishop, D. Rueckert, and Z. Wang, “Real-time single image and video super-resolution using an efficient sub-pixel convolutional neural network,” in *2016 IEEE Conference on Computer Vision and Pattern Recognition (CVPR)*, 2016, pp. 1874–1883.
- [41] Y. Zhang, Y. Tian, Y. Kong, B. Zhong, and Y. Fu, “Residual dense network for image super-resolution,” in *2018 IEEE/CVF Conference on Computer Vision and Pattern Recognition*, 2018, pp. 2472–2481.
- [42] Y. Zhang, K. Li, K. Li, L. Wang, B. Zhong, and Y. Fu, “Image super-resolution using very deep residual channel attention networks,” in *Computer Vision – ECCV 2018*, 2018, pp. 294–310.
- [43] A. Shocher, N. Cohen, and M. Irani, “Zero-shot super-resolution using deep internal learning,” in *2018 IEEE/CVF Conference on Computer Vision and Pattern Recognition*, 2018, pp. 3118–3126.

- [44] C. Ledig, L. Theis, F. Huszar, J. Caballero, A. Cunningham, A. Acosta, A. Aitken, A. Tejani, J. Totz, Z. Wang, and W. Shi, "Photo-realistic single image super-resolution using a generative adversarial network," in *2017 IEEE Conference on Computer Vision and Pattern Recognition (CVPR)*, 2017, pp. 105–114.
- [45] A. Dosovitskiy, P. Fischer, E. Ilg, P. Husser, C. Hazirbas, V. Golkov, P. v. d. Smagt, D. Cremers, and T. Brox, "FlowNet: Learning optical flow with convolutional networks," in *2015 IEEE International Conference on Computer Vision (ICCV)*, 2015, pp. 2758–2766.
- [46] B. D. Lucas and T. Kanade, "An iterative image registration technique with an application to stereo vision," in *Proceedings of the 7th International Joint Conference on Artificial Intelligence*, 1981, pp. 674–679.
- [47] M. Drulea and S. Nedeveschi, "Total variation regularization of local-global optical flow," in *2011 14th International IEEE Conference on Intelligent Transportation Systems (ITSC)*, 2011, pp. 318–323.
- [48] E. Ilg, N. Mayer, T. Saikia, M. Keuper, A. Dosovitskiy, and T. Brox, "FlowNet 2.0: Evolution of optical flow estimation with deep networks," in *2017 IEEE Conference on Computer Vision and Pattern Recognition (CVPR)*, 2017, pp. 1647–1655.
- [49] A. Ranjan and M. J. Black, "Optical flow estimation using a spatial pyramid network," in *2017 IEEE Conference on Computer Vision and Pattern Recognition (CVPR)*, 2017, pp. 2720–2729.
- [50] M. Jaderberg, K. Simonyan, A. Zisserman, and k. kavukcuoglu, "Spatial transformer networks," in *Advances in Neural Information Processing Systems 28*, 2015, pp. 2017–2025.
- [51] T. Brox, A. Bruhn, N. Papenberger, and J. Weickert, "High accuracy optical flow estimation based on a theory for warping," in *Computer Vision - ECCV 2004*, T. Pajdla and J. Matas, Eds., 2004, pp. 25–36.
- [52] C. Liu *et al.*, "Beyond pixels: exploring new representations and applications for motion analysis," Ph.D. dissertation, Massachusetts Institute of Technology, 2009.
- [53] L. Xu, J. Jia, and Y. Matsushita, "Motion detail preserving optical flow estimation," *IEEE Transactions on Pattern Analysis and Machine Intelligence*, vol. 34, no. 9, pp. 1744–1757, Sep. 2012.
- [54] D. P. Kingma and J. Ba, "Adam: A method for stochastic optimization," in *International Conference on Learning Representations (ICLR)*, 2015.
- [55] X. Shi, Z. Chen, H. Wang, D.-Y. Yeung, W.-k. Wong, and W.-c. Woo, "Convolutional LSTM network: A machine learning approach for precipitation nowcasting," in *Advances in Neural Information Processing Systems 28*, 2015, pp. 802–810.
- [56] X. Glorot and Y. Bengio, "Understanding the difficulty of training deep feedforward neural networks," in *Proceedings of the Thirteenth International Conference on Artificial Intelligence and Statistics*, 2010, pp. 249–256.
- [57] O. Ronneberger, P. Fischer, and T. Brox, "U-net: Convolutional networks for biomedical image segmentation," in *Medical Image Computing and Computer-Assisted Intervention – MICCAI 2015*, 2015, pp. 234–241.
- [58] J. Pont-Tuset, F. Perazzi, S. Caelles, P. Arbeláez, A. Sorkine-Hornung, and L. Van Gool, "The 2017 DAVIS Challenge on Video Object Segmentation," *arXiv e-prints*, p. arXiv:1704.00675, Apr 2017.
- [59] G. Huang, Z. Liu, L. Van Der Maaten, and K. Q. Weinberger, "Densely connected convolutional networks," in *2017 IEEE Conference on Computer Vision and Pattern Recognition (CVPR)*, 2017, pp. 2261–2269.
- [60] M. Irani and S. Peleg, "Improving resolution by image registration," *CVGIP: Graphical Models and Image Processing*, vol. 53, no. 3, pp. 231 – 239, 1991.
- [61] "Motion analysis for image enhancement: Resolution, occlusion, and transparency," *Journal of Visual Communication and Image Representation*, vol. 4, no. 4, pp. 324 – 335, 1993.
- [62] M. Haris, G. Shakhnarovich, and N. Ukita, "Deep back-projection networks for super-resolution," in *2018 IEEE Conference on Computer Vision and Pattern Recognition*, 2018, pp. 1664–1673.
- [63] K. He, X. Zhang, S. Ren, and J. Sun, "Deep residual learning for image recognition," in *2016 IEEE Conference on Computer Vision and Pattern Recognition (CVPR)*, 2016, pp. 770–778.
- [64] B. Lim, S. Son, H. Kim, S. Nah, and K. M. Lee, "Enhanced deep residual networks for single image super-resolution," in *2017 IEEE Conference on Computer Vision and Pattern Recognition Workshops (CVPRW)*, 2017, pp. 1132–1140.
- [65] K. Li, B. Bare, B. Yan, B. Feng, and C. Yao, "Face hallucination based on key parts enhancement," in *2018 IEEE International Conference on Acoustics, Speech and Signal Processing (ICASSP)*, 2018, pp. 1378–1382.
- [66] S. Nah, S. Baik, S. Hong, G. Moon, S. Son, R. Timofte, and K. M. Lee, "NTIRE 2019 challenge on video deblurring and super-resolution: Dataset and study," in *2019 IEEE Conference on Computer Vision and Pattern Recognition Workshops (CVPRW)*, 2019, pp. 1996–2005.
- [67] S. Nah, R. Timofte, S. Gu, S. Baik, S. Hong, G. Moon, S. Son, K. M. Lee, X. Wang, K. C. K. Chan, K. Yu, C. Dong, C. C. Loy, Y. Fan, J. Yu, D. Liu, T. S. Huang, X. Liu, C. Li, D. He, Y. Ding, S. Wen, F. Porikli, R. Kalarot, M. Haris, G. Shakhnarovich, N. Ukita, P. Yi, Z. Wang, K. Jiang, J. Jiang, J. Ma, H. Dong, X. Zhang, Z. Hu, K. Kim, D. U. Kang, S. Y. Chun, K. Purohit, A. N. Rajagopalan, Y. Tian, Y. Zhang, Y. Fu, C. Xu, A. M. Tekalp, M. A. Yilmaz, C. Korkmaz, M. Sharma, M. Makwana, A. Badhwar, A. P. Singh, A. Upadhyay, R. Mukhopadhyay, A. Shukla, D. Khanna, A. S. Mandal, S. Chaudhury, S. Miao, Y. Zhu, and X. Huo, "NTIRE 2019 challenge on video super-resolution: Methods and results," in

- 2019 *IEEE Conference on Computer Vision and Pattern Recognition Workshops (CVPRW)*, 2019, pp. 1985–1995.
- [68] J. Dai, H. Qi, Y. Xiong, Y. Li, G. Zhang, H. Hu, and Y. Wei, “Deformable convolutional networks,” in *2017 IEEE International Conference on Computer Vision (ICCV)*, 2017, pp. 764–773.
- [69] X. Zhu, H. Hu, S. Lin, and J. Dai, “Deformable ConvNets V2: More deformable, better results,” in *2019 IEEE Conference on Computer Vision and Pattern Recognition (CVPR)*, 2019, pp. 9300–9308.
- [70] D. Sun, X. Yang, M. Liu, and J. Kautz, “PWC-Net: CNNs for optical flow using pyramid, warping, and cost volume,” in *2018 IEEE Conference on Computer Vision and Pattern Recognition*, 2018, pp. 8934–8943.
- [71] T. Hui, X. Tang, and C. C. Loy, “LiteFlowNet: A lightweight convolutional neural network for optical flow estimation,” in *2018 IEEE Conference on Computer Vision and Pattern Recognition*, 2018, pp. 8981–8989.
- [72] —, “A lightweight optical flow cnn - revisiting data fidelity and regularization,” *IEEE Transactions on Pattern Analysis and Machine Intelligence*, 2020.
- [73] X. Wang, R. Girshick, A. Gupta, and K. He, “Non-local neural networks,” in *2018 IEEE Conference on Computer Vision and Pattern Recognition*, 2018, pp. 7794–7803.
- [74] Z. Hui, J. Li, X. Gao, and X. Wang, “Progressive perception-oriented network for single image super-resolution,” *CoRR*, vol. abs/1907.10399, 2019. [Online]. Available: <http://arxiv.org/abs/1907.10399>
- [75] K. Simonyan and A. Zisserman, “Very deep convolutional networks for large-scale image recognition,” in *Proceedings of the 3rd International Conference on Learning Representations (ICLR)*, 2015.
- [76] D. Tran, L. Bourdev, R. Fergus, L. Torresani, and M. Paluri, “Learning spatiotemporal features with 3d convolutional networks,” in *2015 IEEE International Conference on Computer Vision (ICCV)*, 2015, pp. 4489–4497.
- [77] S. Ji, W. Xu, M. Yang, and K. Yu, “3D convolutional neural networks for human action recognition,” *IEEE Transactions on Pattern Analysis and Machine Intelligence*, vol. 35, no. 1, pp. 221–231, Jan 2013.
- [78] X. Jia, B. De Brabandere, T. Tuytelaars, and L. V. Gool, “Dynamic filter networks,” in *Advances in Neural Information Processing Systems 29*, 2016, pp. 667–675.
- [79] O. Shahar, A. Faktor, and M. Irani, “Space-time super-resolution from a single video,” in *2011 IEEE Conference on Computer Vision and Pattern Recognition*, 2011, pp. 3353–3360.
- [80] S. Hochreiter and J. Schmidhuber, “Long short-term memory,” *Neural Computation*, vol. 9, no. 8, pp. 1735–1780, 1997.
- [81] J.-H. Jacobsen, A. W. Smeulders, and E. Oyallon, “i-RevNet: Deep invertible networks,” in *International Conference on Learning Representations (ICLR)*, 2018.
- [82] J. Kim, J. K. Lee, and K. M. Lee, “Deeply-recursive convolutional network for image super-resolution,” in *2016 IEEE Conference on Computer Vision and Pattern Recognition (CVPR)*, 2016, pp. 1637–1645.
- [83] Y. Tai, J. Yang, and X. Liu, “Image super-resolution via deep recursive residual network,” in *2017 IEEE Conference on Computer Vision and Pattern Recognition (CVPR)*, 2017, pp. 2790–2798.
- [84] J. Chen, X. Tan, C. Shan, S. Liu, and Z. Chen, “Vesr-net: The winning solution to youku video enhancement and super-resolution challenge,” *arXiv preprint arXiv:2003.02115*, 2020.